이학박사 학위논문

Investigation of aerosol effects on regional climate in East Asia using a new chemistry-climate model

새로운 화학-기후 모델을 활용한 동아시아 지역 기후에 대한 에어로졸 효과 연구

2022년 8월

서울대학교 대학원

지구환경과학부

이 승 언

Investigation of aerosol effects on regional climate in East Asia using a new chemistry-climate model

지도 교수 박 록 진

이 논문을 이학박사 학위논문으로 제출함
2022년 4월

서울대학교 대학원
지구환경과학부
이 승 언

이승언의 이학박사 학위논문을 인준함
2022년 6월

위 원 장 김 상 우 (인)

부위원장 박 록 진 (인)

위 원 손 석 우 (인)

위 원 예 상 욱 (인)

위 원 홍 성 유 (인)

Abstract

A new chemistry-climate model, the Global/Regional Integrated Model system Chemistry Climate Model (GRIMs-CCM), is developed by coupling the chemistry modules of the GEOS-Chem chemical transport model to the GRIMs general circulation model. The GRIMs-CCM is driven by meteorological variables simulated by the GRIMs and uses simulated gas and aerosol concentrations to calculate the radiative transfer equations at each time step. The model is evaluated by comparing ozone and aerosol concentrations with respective observations from the surface networks and the satellite datasets. It is found that the GRIMs-CCM successfully reproduces the observed spatial distributions of annual-mean aerosol optical depth and captures the seasonal and latitudinal variations of total column ozone. The evaluation of simulated aerosols in surface air against the observations reveals that the model reproduces the observed temporal and spatial variations but shows biases in soil dust aerosols. I also estimate the climatic impact of aerosols by conducting two sets of 10-year simulations

for the preindustrial and present conditions. The GRIMs-CCM shows the aerosol radiative forcing of −0.30 W m^{-2} from the preindustrial to present-day climates, comparable to the values from other climate model intercomparison projects. These results suggest that the GRIMs-CCM is suitable for studying chemistry-climate interactions and their changes over time. I investigate the regional climatic impact of aerosols in East Asia by conducting sensitivity analyses using the GRIMs-CCM and Community Earth System Model (CESM). I conduct 20 ensembles of 7-year simulations prescribing a recently decreasing trend of aerosol optical depth in East Asia observed from the satellite measurements to the models. It is found that the ensemble means of GRIMs-CCM and CESM reproduce positive trends of recent wintertime surface temperature in East Asia shown in the ERA-Interim reanalysis data. Comparisons of model results with the sensitivity simulations with detrended aerosol optical depth show that the models with decreasing aerosol optical depth simulate stronger warming trends in surface temperature, which indicates that the recent reduction of aerosols in East Asia partly contributes to the positive trends in surface temperature in East Asia.

Keywords: Chemistry-climate model, Aerosol, Ozone,

Aerosol radiative forcing, GRIMs, GEOS-Chem

Student Number: 2012-20345

Table of Contents

List of Tables

List of Figures

1. Introduction

Short-lived climate pollutants (SLCPs) have been under extensive scrutiny for their roles in perturbing the Earth's radiation balance (Charlson et al., 1992; Hansen et al., 1997; Haywood and Boucher, 2000; Naik et al., 2013; Shindell et al., 2008; Stohl et al., 2015). They include methane, tropospheric ozone, hydrofluorocarbons, and black carbon aerosol, which mainly exert positive radiative forcing on the earth system. Other components of tropospheric aerosols, such as sulfate, nitrate, ammonium, and organic aerosols, which are not classified as SLCPs, also play an essential role in affecting climate by scattering solar radiation. Moreover, tropospheric aerosols act as ice or cloud condensation nuclei and thus change the cloud albedo or lifetime (Lohmann and Feichter, 2005; Quaas et al., 2009; Tao et al., 2012), which is referred to as the aerosol-cloud interaction and causes significant uncertainty in future climate projections (Intergovernmental Panel on Climate Change, 2013; Shindell et al., 2013).

The 6th Assessment Report of the Intergovernmental Panel on

Climate Change (Forster et al., 2021) reported that the effective radiative forcing (radiative forcing with adjustment of atmospheric state by the climate forcing agent) of aerosols for the period of 1750–2019 due to both the aerosol-radiation interaction and the aerosol-cloud interaction is −1.06 W m^{-2} (−1.92 to −0.21). The ozone radiative forcing for the same period is +0.47 W m^{-2} (+0.24 to +0.71). The total radiative forcing of aerosols and ozone is 1.53 W m^{-2}, nearly half of the radiative forcing of the well-mixed greenhouse gases (GHGs), 3.32 W m^{-2} (+2.84 to +3.79). While the GHGs are chemically less reactive and evenly distributed globally, the SLCPs and other tropospheric aerosols have short lifetimes of a few days or weeks in the atmosphere except for CH_4. They are distributed unevenly around the globe, having significant implications for regional climate (Shindell et al., 2013). The complex and nonlinear aerosol-cloud interactions make the estimate of aerosol radiative forcing even more uncertain (Lohmann et al., 2010; Myhre et al., 2013). For instance, the uncertainty of the radiative forcing of SLCPs is 4 to 5 times higher than that of GHGs (Intergovernmental Panel on Climate Change, 2013). Hence, it is crucial to better understand the physical and chemical processes involved in the

SLCPs and tropospheric aerosol formations and their interactions with the climate system to reduce the uncertainty of the anthropogenic radiative forcing for future climate projections.

Exploring the chemistry-climate interactions can be fulfilled by using a coupled chemistry-climate model, which explicitly simulates the complex atmospheric chemistry processes and their interactions with the climate system. Due to recent advances in the computation power and parallelization technique, many chemistry-climate models have been developed (Morgenstern et al., 2017; Shindell et al., 2013). They have varying complexity in simulating atmospheric chemistry processes, resulting in significant gaps in estimating the radiative forcing of SLCPs (Myhre et al., 2013; Shindell et al., 2013). Several model intercomparison projects, including the Atmospheric Chemistry and Climate Model Intercomparison Project (ACCMIP) (Lamarque et al., 2013), Chemistry-Climate Model Initiative (CCMI) (Morgenstern et al., 2017), and Coupled Model Intercomparison Project Phase 6 (CMIP6) (Eyring et al., 2016), were conducted to divulge associated uncertainties with coupled chemistry-climate simulations of participating models. The model intercomparisons

revealed that the multi-model means are consistent with the present-day observations. Still, the model spreads appear large, indicating significant model uncertainties in simulating chemistry-climate interactions.

This dissertation introduces a new global atmospheric chemistry-climate model, the Global/Regional Integrated Model system Chemistry Climate Model (GRIMs-CCM), developed by coupling the GRIMs general circulation model and GEOS-Chem chemical transport model. The GRIMs is a multiscale seamless atmospheric general circulation model, and its capability of reproducing the climatological mean state of the atmosphere is thoroughly validated by a previous study (Hong et al., 2013). The GEOS-Chem has been widely used and extensively evaluated in the literature, and it is well received that the GEOS-Chem can reproduce the spatial and temporal variability of the SLCPs and other tropospheric aerosols (Bey et al., 2001; Jeong and Park, 2017; Jo et al., 2016; Kim et al., 2015; Park et al., 2004).

This dissertation presents the general description of the GRIMs-CCM and then evaluates its performance by comparing the simulated chemical species, focusing on aerosol components and ozone, with observations from

satellite and surface networks. I also estimate the radiative forcing of aerosols by conducting time-scale experiments using GRIMs-CCM and compare the result with the values from the chemistry-climate models in the literature as an indirect evaluation of the model's capability to simulate the radiative forcing of SLCPs. Finally, I investigate the climatic impact of aerosols by prescribing a recently decreasing trend of aerosol optical depth in East Asia to the GRIMs-CCM.

2. Model Description

2.1. Atmospheric General Circulation Model

The GRIMs is a multiscale atmospheric model system developed for numerical weather prediction and climate studies from regional to global scales (Chang et al., 2013; Hong et al., 2013; Lee et al., 2014). It consists of global/regional atmospheric and ocean models, a single column model, and a data assimilation package. As an atmospheric model component of the GRIMs-CCM, I employ the GRIMs-global model program with a spectral dynamic core using spherical harmonics as a basis function. To avoid the Gibbs phenomenon due to spectral transform, I used a semi-Lagrangian scheme to simulate the advection of hydrometeors (Koo et al., 2022). The default horizontal resolution of the model is T62 spectral truncation, which is equivalent to about a 210 km resolution at the equator and corresponds to 192 x 94 (longitude, latitude) gaussian grids. The default number of vertical layers is 47 in a hybrid sigma-pressure coordinate system, the top of which is 0.01 hPa. The model uses a semi-implicit time integration scheme with a

timestep of 20-minute. Note that the user customizes the horizontal and vertical resolutions to fit the spatial and temporal scope of research interests.

Physics schemes are based on the GRIMs physics package v3.1, thoroughly described and evaluated by Hong et al. (2013). In the GRIMs-CCM, the shortwave and longwave radiation schemes are replaced with the widely used Rapid Radiative Transfer Model for general circulation model (RRTMG) to facilitate the interaction of the radiation and chemical tracers (Clough et al., 2005; Mlawer et al., 1997). The cumulus parameterization scheme is changed to the simplified Arakawa-Schubert scheme developed for the Korean Integrated Model (Han et al., 2020; Hong et al., 2018), which is an updated version of the convection scheme used in the National Centers for Environmental Prediction (NCEP) Global Forecast System (Han and Pan, 2011), to improve the sub-grid scale convective transport of chemical tracers. All the references for individual schemes used in the GRIMs-CCM are summarized in **Table 2.1**.

Table 2.1. Overview of GRIMs-CCM model components and their references.

Based General Circulation Model	GRIMs	Hong et al. 2013
Advection	Semi-Lagrangian	Koo et al. 2022
Radiation	RRTMG	Clough et al. 2005; Mlawer et al. 1997
Cumulus	Simplified Arakawa-Schubert scheme for KIM	Han et al. 2020; Hong et al. 2018
Other Physics	GRIMs physics package v3.1	Hong et al. 2013
Based Chemical Transport Model	GEOS-Chem v9-01-02	Bey et al. 2001
Dry Deposition	Resistance-in-series model	Wesely 1989; Zhang et al. 2001
Wet Deposition	Large-scale & Convective scavenging	Liu et al. 2001
Photolysis	FAST-J scheme	Wild et al. 2000
Chemistry Solver	KPP; SMVGEAR II	Damian et al. 2002; Jacobson 1995
Heterogeneous Chemistry	Reactive uptake coefficients	Evans and Jacob 2005; Jacob 2000
Stratospheric Ozone	LINOZ	McLinden et al. 2000
Tropospheric Aerosols	Sulfate-Nitrate-Ammonium; BC; OC; Dust; Sea-salt	Alexander et al. 2005; Fairlie et al. 2007; Park et al. 2003, 2004
PBL mixing	TURBDAY; VDIFF	Lin and McElroy 2010

2.2. Chemistry Modules

The chemistry modules are obtained from the GEOS-Chem v9-01-02 (http://www.geos-chem.org) with several modifications in the source code structure. The GEOS-Chem is an offline 3-dimensional global chemical transport model driven by archived assimilated meteorological data from the Goddard Earth Observation System (GEOS) of the NASA Global Modeling and Assimilation Office (GMAO). The source codes of the GEOS-Chem are modified as subordinate modules of the GRIMs, and the chemistry modules are then driven by simulated meteorology every timestep. The model calculates the emission, deposition, chemistry, and transport processes of 43 chemical tracers, including NO_X, O_X, CO, non-methane volatile organic compounds (NMVOCs), and aerosol species (**Table 2.2**). Some details are described below.

Table 2.2. List of chemical tracers in the chemistry module.

Tracer Name	Description
NO_X	$NO + NO_2 + NO_3 + HNO_2$
O_X	$O_3 + NO_2 + 2NO_3$
PAN	Peroxyacetyl Nitrate
CO	Carbon Monoxide
ALK4	Lumped Alkanes >= C_4
ISOP	Isoprene
HNO_3	Nitric Acid
H_2O_2	Hydrogen Peroxide
ACET	Acetone
MEK	Methyl Ethyl Ketone
ALD2	Acetaldehyde
RCHO	Lumped Aldehydes >= C_3
MVK	Methyl Vinyl Ketone
MACR	Methacrolein
PMN	Peroxymethacroyl Nitrate
PPN	Peroxypropionyl Nitrate
R4N2	Lumped Alkyl Nitrate
PRPE	Lumped Alkenes >= C_3
C_3H_8	Propane
CH_2O	Formaldehyde
C_2H_6	Ethane
N_2O_5	Dinitrogen Pentoxide
HNO_4	Pernitric Acid
MP	Methyl Hydro Peroxide
DMS	Dimethyl Sulfide
SO_2	Sulfur Dioxide
SO_4	Sulfate
SO_4s	Sulfate on surface of sea salt aerosol
MSA	Methyl Sulfonic Acid
NH_3	Ammonia
NH_4	Ammonium
NIT	Inorganic nitrates
NITs	Inorganic nitrates on surface of sea salt aerosol
BCPI	Hydrophilic black carbon aerosol
OCPI	Hydrophilic organic carbon aerosol
BCPO	Hydrophobic black carbon aerosol
OCPO	Hydrophobic organic carbon aerosol
DST1	Dust aerosol, R_{eff} = 0.7 microns
DST2	Dust aerosol, R_{eff} = 1.4 microns
DST3	Dust aerosol, R_{eff} = 2.4 microns
DST4	Dust aerosol, R_{eff} = 4.5 microns
SALA	Accumulation mode sea salt aerosol
SALC	Coarse mode sea salt aerosol

(a) Emissions

The global anthropogenic emissions of CO, NO_X, and SO_2 are taken from the Emission Database for Global Atmospheric Research (EDGAR) global emission inventory (Olivier et al., 1996). If up-to-dated regional anthropogenic emission inventories are available, they are superseded regionally over EDGAR emissions. They include the data from the European Monitoring and Evaluation Programme (EMEP) for Europe, the Big Bend Regional Aerosol and Visibility Observational Study (BRAVO) for Mexico, the Intercontinental Chemical Transport Experiment-Phase B (INTEX-B) for East Asia, the Criteria Air Contaminants (CAC) for Canada, and the National Emission Inventory 2005 (NEI2005) for the United States (Kuhns et al., 2005; van Donkelaar et al., 2008; Zhang et al., 2009).

Anthropogenic emissions of NMVOCs are obtained from the Reanalysis of the Tropospheric Chemical Composition over the past 40 years (RETRO) global emission inventory (Pulles et al., 2007). The aircraft NO_X emission is taken from the Aviation Emissions Inventory Code (AEIC) inventory (Stettler et al., 2011), while the soil NO_X emissions are calculated following the algorithm of Yienger and Levy (1995). The lightning NO_X

emissions are calculated based on the temperature profile and the depth of convective clouds from the GCM, as described in Murray et al. (2012). The volcanic SO_2 emissions from the eruptive and non-eruptive volcanoes are taken from the Aerosol Comparisons between Observations and Models (AEROCOM) database. The emissions from biomass burning are obtained from the Global Fire Emissions Database version 3 (GFED3) monthly database (van der Werf et al., 2010). The biogenic emissions of NMVOCs, including isoprene and monoterpenes, are calculated from the Model of Emissions of Gases and Aerosols from Nature version 2.1 (MEGANv2.1) using meteorological variables from the online coupled GCM (Guenther et al., 2012). The anthropogenic emissions of primary carbonaceous aerosols are taken from Bond et al. (2007). The natural emission of soil dust aerosols is calculated using either the Goddard Chemistry Aerosol Radiation and Transport (GOCART) scheme (Ginoux et al., 2004) or the Dust Entrainment and Deposition (DEAD) scheme (Zender et al., 2003), as described in Fairlie et al. (2007). The emission of sea salt aerosols from the ocean is parameterized as a function of surface wind speed following the algorithm of Monahan et al. (1986).

(b) Deposition

The removal processes of chemical tracers by deposition include dry deposition in the planetary boundary layer and wet deposition by precipitation. The dry deposition is calculated based on a resistance-in-series model (Wesely, 1989) with an updated surface resistance for aerosol particles (Zhang et al., 2001). The dry deposition velocity of aerosol particles over snow or ice is set to 0.03 cm s^{-1} (Fisher et al., 2011). The gravitational settling of coarse-mode sea salt aerosols (Alexander et al., 2005) and soil dust aerosols (Fairlie et al., 2007) are also considered in the model. The wet deposition of water-soluble chemical tracers includes in-cloud rainout and below-cloud washout due to large-scale precipitation and scavenging of soluble tracers due to convective updrafts (Liu et al., 2001).

(c) Chemistry

The model calculates 111 chemical species concentrations in every grid cell in the troposphere. The chemical mechanism includes coupled oxidants (O_X-NO_X-NMVOCs)-aerosol chemistry in the troposphere, with 285 gas-phase kinetic reactions, 51 photolysis reactions, and four heterogeneous reactions. The reaction coefficients for gas-phase kinetic reactions are calculated in every grid cell using local pressure and temperature from the atmospheric model. The photolysis rate is calculated using the FAST-J scheme (Wild et al., 2000) by assuming an approximate random cloud overlap (Liu et al., 2006). The reactive uptake coefficients for the heterogeneous reactions are taken from Jacob (2000) except for N_2O_5 hydrolysis, the coefficient of which is from Evans and Jacob (2005). The absorption cross-sections and surface areas of aerosols used for the photolysis and heterogeneous reactions are calculated online using simulated aerosol concentrations assuming the log-normal size distribution. As a default, the Kinetic Preprocessor (KPP) chemistry solver solves the mass balance equations of the reactions (Damian et al., 2002). The SMVGEAR II chemistry solver is an alternative for solving the equation

with relatively slow computation speed but high accuracy (Jacobson, 1995).

In the stratosphere, a simple chemistry process is utilized. Stratospheric ozone is calculated using a simple linearized ozone parameterization (LINOZ) from McLinden et al. (2000). The LINOZ is a first-order Taylor expansion of local ozone due to its concentration, temperature, and overhead column ozone. The net production rates of stratospheric NO_X and HNO_3 are prescribed as climatological mean values. The loss of NMVOCs due to OH radical in the stratosphere is calculated using the climatological stratospheric OH concentration. The tropopause height is calculated following the method in Reichler et al. (2003).

The simulation of inorganic sulfate-nitrate-ammonium (SNA) aerosols is thoroughly described in Park et al. (2004). The sulfur oxidation chemistry includes the gas-phase oxidation of SO_2 by OH radical and in-cloud aqueous-phase oxidation of SO_2 by H_2O_2 and O_3 to produce sulfate aerosol. The nitrate and ammonium aerosol concentrations are determined by calculating thermodynamic equilibrium using the ISORROPIA II module (Fountoukis and Nenes, 2007). The simulation of carbonaceous aerosols is as described in Park et al. (2003). The carbonaceous aerosols include

hydrophilic and hydrophobic black carbon (BC) and organic carbon (OC). It is assumed that 20% of primary BC emission and 50% of primary OC emission are emitted as hydrophilic, whereas the rest of the emission is emitted as hydrophobic. The hydrophobic carbonaceous aerosols are converted to hydrophilic aerosols with an e-folding time of 1.15 days. The secondary organic aerosols (SOA) from biogenic sources are entirely hydrophilic, assuming 10% yields of SOA from total monoterpene emissions. Fairlie et al. (2007) describes the simulation of dust aerosols, and Alexander et al. (2005) describe the simulation of sea salt aerosols in detail.

(d) Transport

The GEOS-Chem uses TPCORE as an advection algorithm for the chemical tracers (Lin and Rood, 1996). In GRIMs-CCM, TPCORE is replaced with the semi-Lagrangian scheme used for the advection of hydrometeors in the GCM for the dynamical consistency. The vertical transport of chemical tracers due to sub-grid convective updrafts and associated horizontal advection of lifted chemical tracers can be a source of large uncertainty in the model (Pouyaei et al., 2021). GRIMs-CCM accounts for updraft, downdraft, entrainment, and detrainment processes of cumulus convection to better represent sub-grid scale convective transport by implementing a scale-aware and physics-based cumulus scheme (Han et al., 2020). For the turbulent mixing of chemical tracers in the boundary layer, either a full boundary layer mixing scheme (TURBDAY) or a non-local boundary layer mixing scheme (VDIFF) (Lin and McElroy, 2010) can be used for the turbulent mixing of chemical tracers within the boundary layer.

2.3. Coupling Chemical Processes to GRIMs

Figure 2.1 shows a schematic diagram of individual processes in the GRIMs-CCM, indicating that simulated meteorological variables from the atmospheric model drive a chemistry simulation. The 3-D ozone and aerosol concentrations and their optical properties are used as input for the radiative transfer calculation in the atmospheric model. The chemistry module is called every timestep with updated meteorological variables. The ozone concentration and aerosol optical properties are transferred to the atmospheric model when the radiative transfer calculation is conducted (typically once per hour). Here aerosol optical properties include aerosol optical depth (AOD), single scattering albedo, and asymmetry parameters. The optical properties of individual aerosol species, including sulfate, OC, BC, sea salt, and soil dust aerosols, are calculated with the MIE theory as a function of 14 shortwave wavelength bands and 16 longwave wavelength bands of the RRTMG (Mishchenko et al., 2002). The dust aerosol size distribution is assumed to follow the gamma distribution, while that of the other aerosol species is assumed to follow the log-normal distribution. The

parameters that determine the size distributions' shape are mainly taken from the Optical Properties of Aerosols and Clouds (OPAC) (Hess et al., 1998), as summarized in **Table 2.3**. The refractive indices of dust aerosols are adopted from Sinyuk et al. (2003) and others from Hess et al. (1998). The aerosol hygroscopic growth factor as a function of the relative humidity is obtained from Chin et al. (2002) for BC and Hess et al. (1998) for the other aerosols.

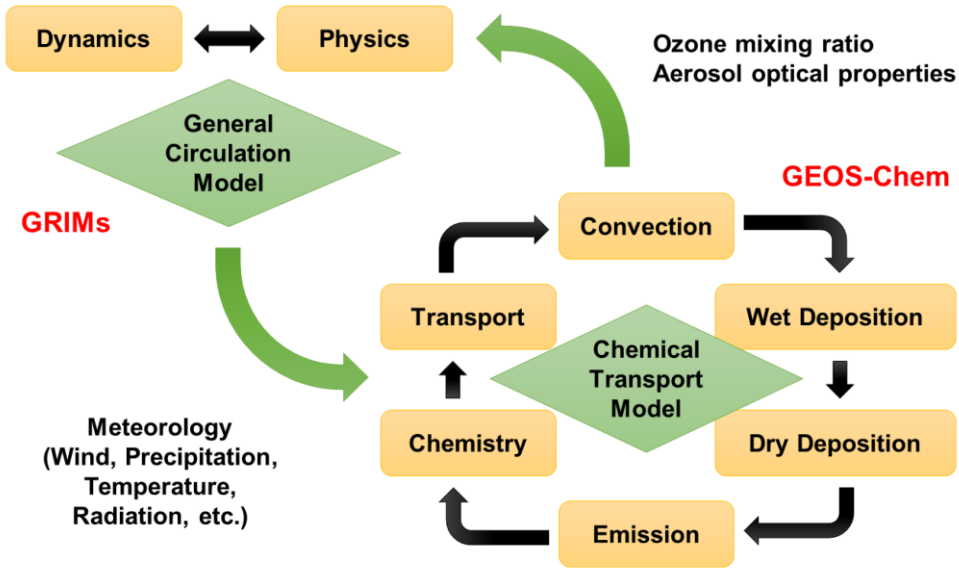

Figure 2.1. Schematic diagram of the structure of GRIMs-CCM.

Table 2.3. Size distribution parameters of the aerosol species (RH=0).

Species	Density (g/cm^3)	Radius (μm)	σ	gam_a	gam_b	r_{min} (μm)	r_{max} (μm)
Sulfate	1.7	0.0695	1.6			0.005	[a]0.5
OC	1.8	[b]0.063	1.6			0.005	[a]0.5
BC	1.0	0.02	1.6			0.005	20
Sea salt (accm.)	2.2	[c]0.085	1.5			0.005	20
Sea salt (coarse.)	2.2	[c]0.4	1.8			0.005	60
Dust (bin 1)	2.5			0.9	0.2	0.1	0.18
Dust (bin 2)	2.5			0.9	0.2	0.18	0.3
Dust (bin 3)	2.5			0.9	0.2	0.3	0.49
Dust (bin 4)	2.5			0.9	0.2	0.65	1.0
Dust (bin 5)	2.65			0.9	0.2	1.3	1.8
Dust (bin 6)	2.65			0.9	0.2	2.2	3.0
Dust (bin 7)	2.65			0.9	0.2	3.5	6.0

[a]Chin et al. (2002)
[b]Drury et al. (2010)
[c]Jaeglé et al. (2011)

3. Model Evaluation

I evaluate the GRIMs-CCM by conducting a 1-year simulation for 2005 after a 1-year spin-up simulation from 2004. The default emission inventories included in the current version of GRIMs-CCM provides the emission data for 2005. The NCEP-DOE AMIP-II Reanalysis (R-2) data (Kanamitsu et al., 2002) are used for the initial condition of the atmospheric model, and the sea surface temperature (SST) and sea-ice concentration are forced by the Global sea-Ice and SST (GISST) data (Rayner et al., 1996) every 24 hours. For land cover data, the hybrid STATSGO-FAO soil texture, U.S. Geological Survey (USGS) global land use, and green vegetation fractions climatology from National Environmental Satellite, Data, and Information Service (NESDIS) (Gutman and Ignatov, 1998) are used. For emissions, the default anthropogenic emission inventories are adopted as described in section 2.2. A non-local mixing scheme (VDIFF) is used for turbulent mixing of chemical tracers within the planetary boundary layer, while a KPP chemistry solver is used for solving the mass balance equations

of the chemistry mechanism.

I additionally conduct a GEOS-Chem simulation for the same period as a reference. The GEOS-Chem simulation is driven by GEOS-5 assimilated meteorological data with 2°x2.5° horizontal resolutions. The number of vertical layers in the GEOS-Chem simulation is identical to the GRIMs-CCM simulation, and the same anthropogenic emission inventories with identical chemical mechanisms to GRIMs-CCM are used. The significant difference between the two simulations is that the GEOS-Chem simulation is driven by assimilated meteorological data, i.e., offline run, while the GRIMs-CCM simulation is driven by the meteorological variables calculated from the online atmospheric model. Their difference mainly indicates the importance of meteorological fields and interactive coupling.

The natural emissions of soil dust and sea salt aerosols are highly sensitive to the surface wind speed, so the natural emissions from the two models are likely to be different as the two models use different meteorology. Thus, scale factors are applied to the soil dust and sea salt emissions for the GRIMs-CCM to assure the two models have the same annual global emissions. As the model performance of reproducing the

climatological mean state of the atmosphere is already validated in previous studies (Hong et al., 2013; Jeong et al., 2019), I focus on the evaluation of the chemistry module by comparing simulated AOD, ozone, and surface particulate matters from the GRIMs-CCM and the GEOS-Chem with the satellite or in-situ measurements below.

3.1. Aerosol Optical Depth

I first evaluate the 550 nm AOD in terms of global distribution compared to the satellite measurement. I use the standard product of Terra/Aqua Moderate Resolution Imaging Spectroradiometer (MODIS) level 3 monthly 1°x1° gridded data (MOD08_M3, MYD08_M3) (Levy et al., 2013; Remer et al., 2005) together with the MODIS AOD retrieved from Deep Blue algorithm (Hsu et al., 2006; Sayer et al., 2013) for infilling missing data over the bright surface, which are averaged from 2004 to 2006.

Figure 3.1 shows the spatial distribution of annual-mean AOD from the observation, GRIMs-CCM, and GEOS-Chem. The MODIS observation shows a high amount of 550 nm AOD over East Asia, northern Africa, and the southern boundary of Tibet. The spatial distribution of AOD is well captured in the GRIMs-CCM, including high AOD over northern Africa due to dust aerosols from the Sahara Desert and an elevated AOD band over the Southern Ocean due to sea salt aerosols. The GRIMs-CCM also captures the high AOD due to anthropogenic aerosols over East Asia and Indo-Gangetic

Plain. However, the high AODs over Amazon and Central Africa in the satellite measurements are not captured, indicating that the model underestimates primary carbonaceous aerosols from the biomass burning and the secondary organic aerosols from the biogenic VOC emissions over that region.

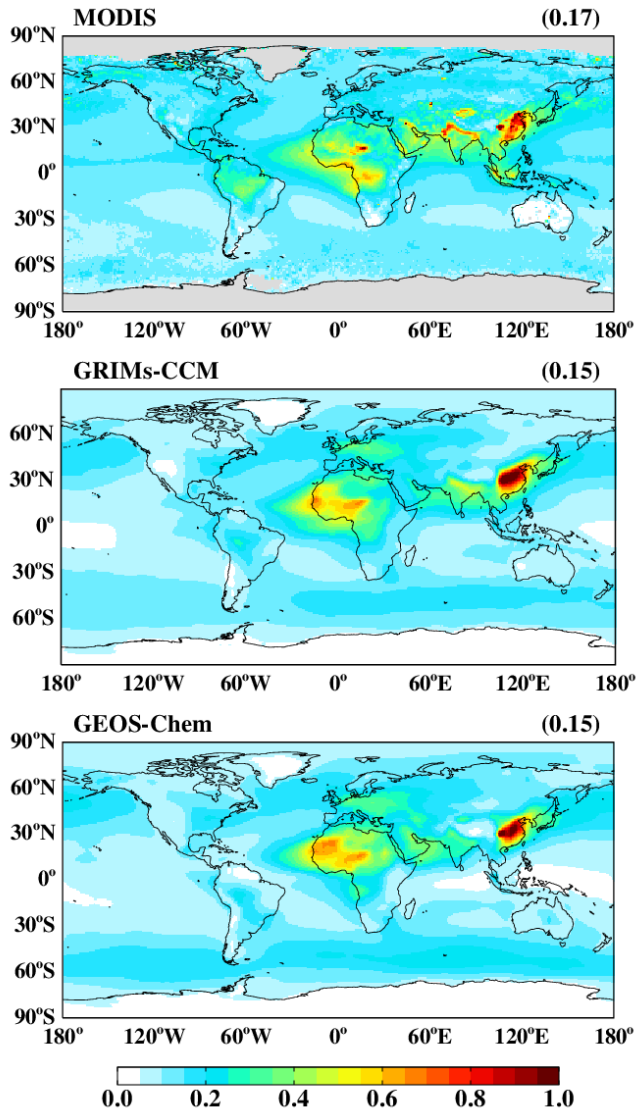

Figure 3.1. Annual mean aerosol optical depth at 550 nm retrieved from the **(top)** MODIS and simulated from the **(middle)** GRIMs-CCM and **(bottom)** GEOS-Chem. The global mean values are shown in the parenthesis in the upper right corner. Gray-shaded indicates the missing data in the MODIS observation.

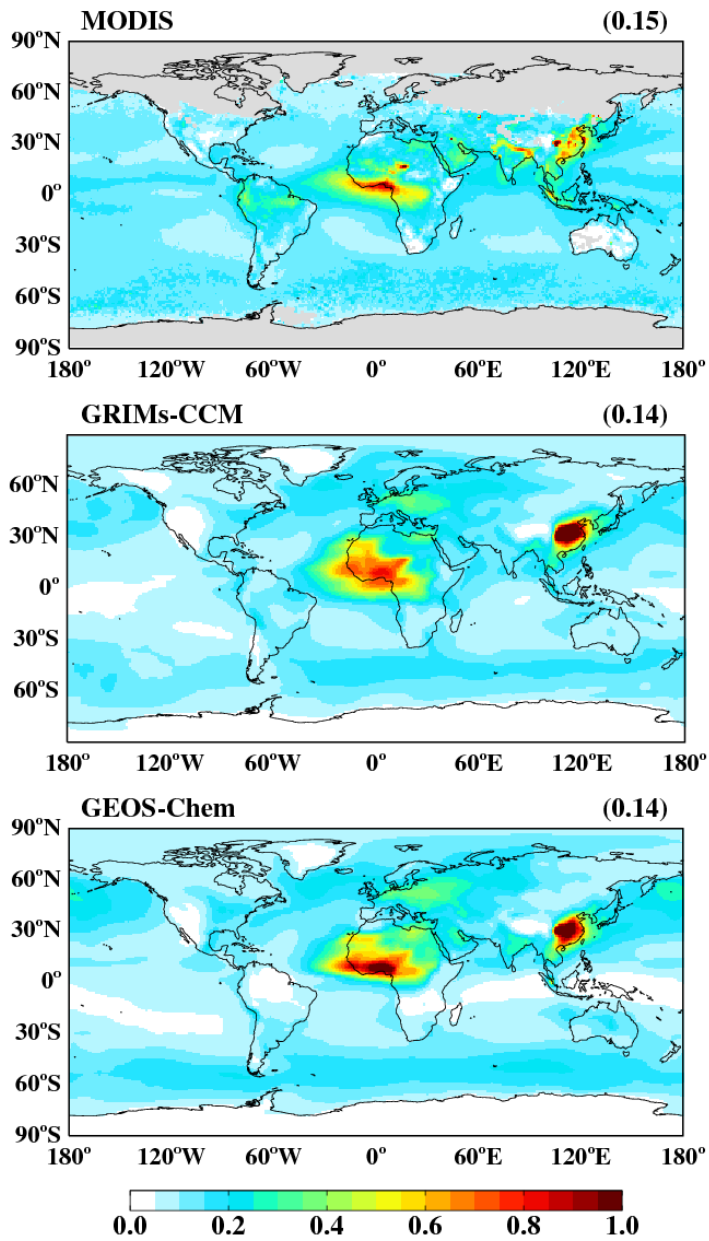

Figure 3.2. Same as **Figure 3.1** but for December–January–February season.

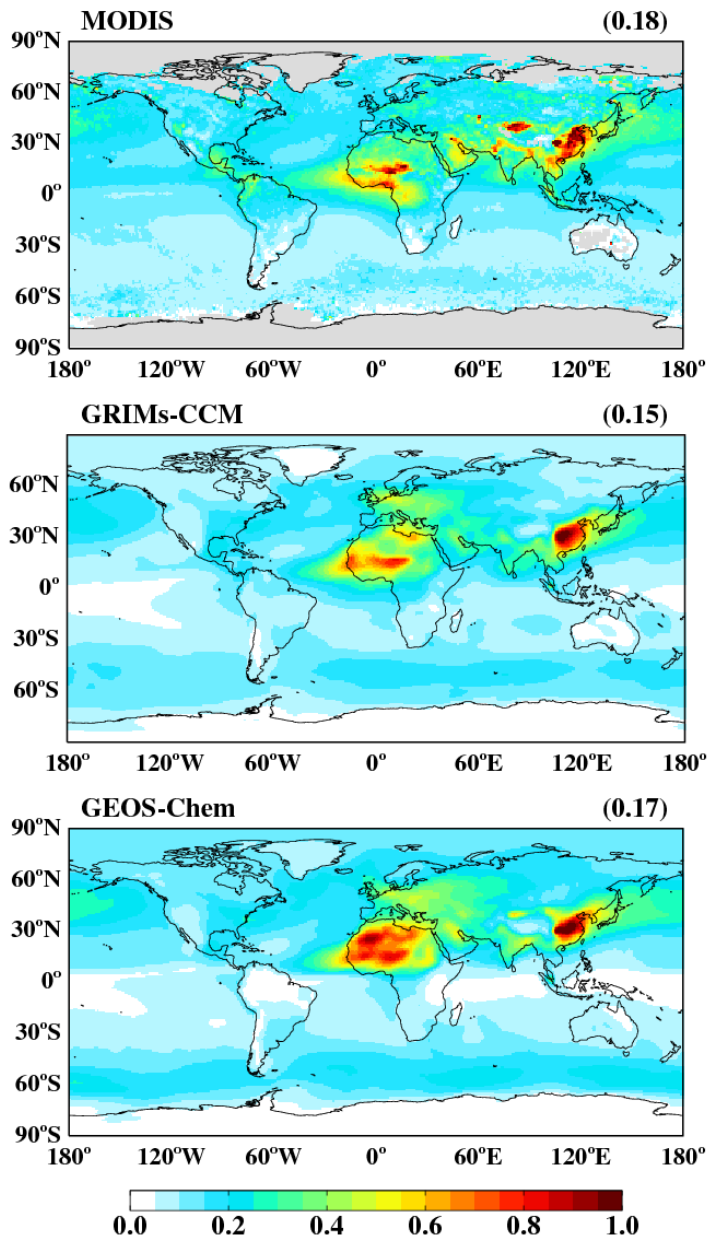

Figure 3.3. Same as **Figure 3.1** but for March–April–May season.

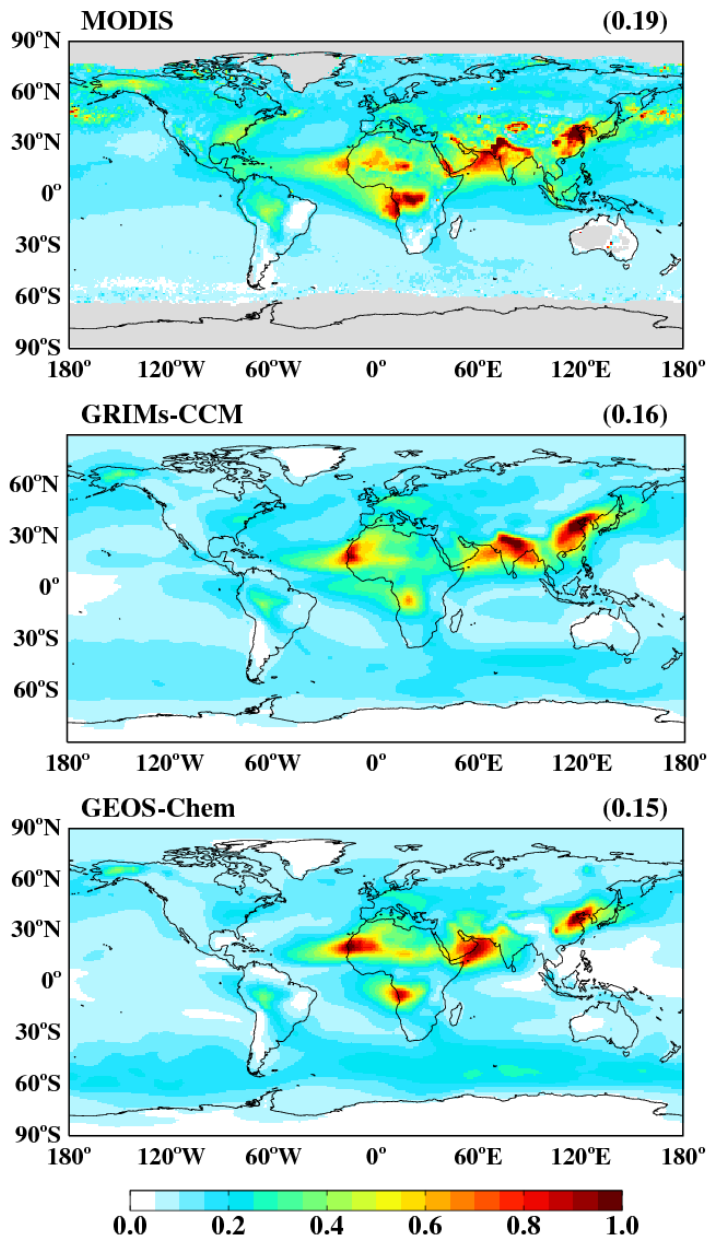

Figure 3.4. Same as **Figure 3.1** but for Jun–July–August season.

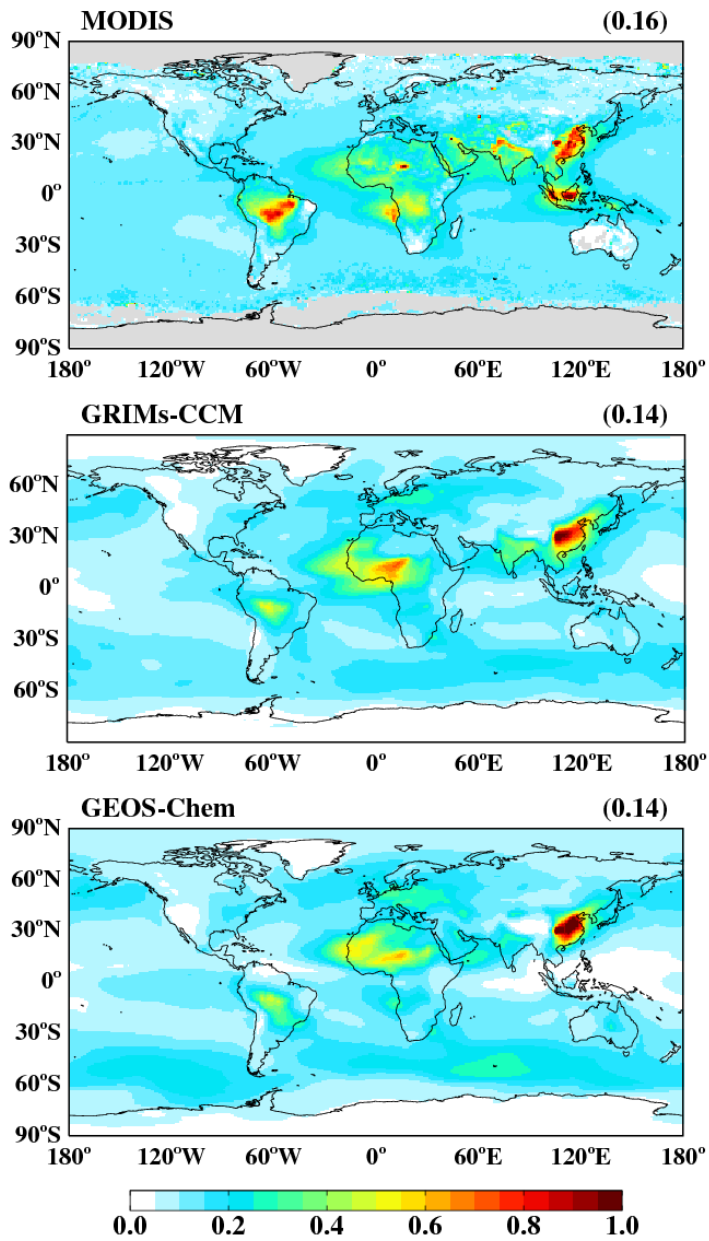

Figure 3.5. Same as **Figure 3.1** but for September–October–November season.

The zonally averaged AOD of different aerosol species is shown in **Figure 3.6**. The observation shows the maximum AOD near 30°N and a secondary peak in the 30°S–60°S latitude band. Both GRIMs-CCM and GEOS-Chem well reproduce the distribution of AOD. In the Southern Hemisphere, the sea salt AOD is responsible for the secondary peak in the 30°S–60°S latitude band, while both dust AOD (0°N–30°N) and sulfate AOD (30°N–60°N) are mainly contributing to high AOD in the Northern Hemisphere.

The correlation coefficient and relative bias of the simulated AOD are quantified at 1° horizontal resolution against the satellite measurements (**Table 3.1**). The correlation coefficient of annual-mean AOD with the observation is 0.65 for the GRIMs-CCM and 0.56 for the GEOS-Chem, which are comparable with those of the ACCMIP models (0.46 to 0.64) reported in Shindell et al. (2013). This indicates that the GRIMs-CCM reasonably reproduces the observed spatial variability of AOD. The bias is −19% for the GRIMs-CCM and −11% for the GEOS-Chem, which are also in the range of the biases from the ACCMIP models (−28% to +54%). Despite using the same emission inventories and chemical mechanisms, the

GRIMs-CCM shows lower AOD than the GEOS-Chem. **Table 3.2** shows aerosol budget analysis of each model, indicating that the GRIMs-CCM has shorter lifetimes of aerosols than the GEOS-Chem due to larger wet and dry deposition losses in the GRIMs-CCM. For example, the GRIMs-CCM calculates higher loss frequencies of aerosols due to wet deposition (+32% for sulfate, +6% for soil dust, +14% for sea salt) and dry deposition (+35% for sulfate, +33% for soil dust, +67% for sea salt) than the GEOS-Chem, implying faster removal of aerosols. The faster deposition in the GRIMs-CCM is likely due to strong cumulus convection and surface friction velocity in the model, which increases the chance of aerosol scavenging in the convective updrafts and the chance of particles touching down the surface, resulting in a higher deposition velocity in the model.

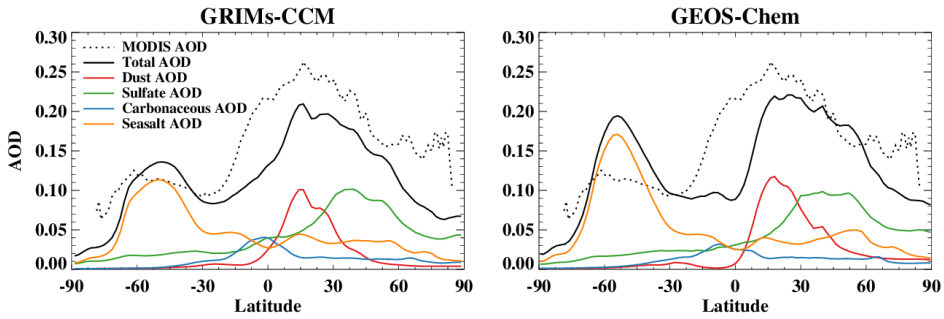

Figure 3.6. Zonally averaged annual mean aerosol optical depth for each aerosol species simulated by the **(left)** GRIMs-CCM and **(right)** GEOS-Chem. The MODIS observation is shown in a black dotted line as a reference. The total AOD (black) is the sum of dust AOD (red), sulfate AOD (green), carbonaceous AOD (sky blue), and sea salt AOD (orange).

Table 3.1. Statistics for the comparison of simulated AOD with the satellite measurement.

Season	GRIMs-CCM		GEOS-Chem	
	r	Bias (%)	r	Bias (%)
Annual	0.65	-19	0.56	-11
DJF	0.63	-17	0.55	-5
MAM	0.69	-21	0.60	-6
JJA	0.70	-21	0.60	-20
SON	0.55	-18	0.49	-9

Table 3.2. Comparison of loss processes for sulfate, dust, and sea salt aerosols in the GRIMs-CCM and the GEOS-Chem.

Component	GRIMs-CCM			GEOS-Chem		
	Sulfate	Dust	Sea salt	Sulfate	Dust	Sea salt
Burden [Tg]	1.51	17.13	4.82	1.80	20.99	5.73
Total deposition [Tg yr^{-1}]	138.3	676.9	1612.2	125.2	776.5	1664.4
Wet deposition	123.7	654.2	1585.6	112.1	757.0	1646.5
Dry deposition	14.58	22.69	26.70	13.06	19.48	17.89
Loss frequency [day^{-1}]						
Wet deposition	0.225	0.105	0.901	0.170	0.099	0.788
Dry deposition	0.027	0.004	0.015	0.020	0.003	0.009
Lifetime [days]	3.97	9.24	1.09	5.26	9.87	1.26

3.2. Ozone

I compare the total column ozone from the model simulations with the satellite measurements. The Aura OMI TOMS-Like Ozone level 3 daily 1°x1° gridded data (OMTO3d) (Balis et al., 2007; Veefkind et al., 2006) is used as an observation for 2005. **Figure 3.7** shows the seasonal variation of zonally averaged total column ozone from the observation, the GRIMs-CCM, and the GEOS-Chem. In the observation, the higher amount of total column ozone is found in high latitudes, indicative of the ozone transport from the tropics to high latitudes through the Brewer-Dobson circulation. The enhancement of total column ozone in the mid-latitudes is shown during the spring season of each hemisphere. The ozone hole in the polar cap of the Southern Hemisphere is also evident in spring (blue in **Fig. 3.7 left**). These seasonal and latitudinal variations are qualitatively reproduced by the GRIMs-CCM and the GEOS-Chem, with a significant underestimation of the Antarctic ozone hole. The LINOZ scheme (McLinden et al., 2000), used to simulate stratospheric ozone in the GRIMs-CCM and the GEOS-Chem, only considers the local tendency as a function

of local ozone mixing ratio, temperature, and overhead column ozone. It misses the complex halogen chemistry responsible for the Antarctic ozone hole. Likewise, it is also difficult to simulate the historical trend of total column ozone due to the changes in ozone-depleting substances.

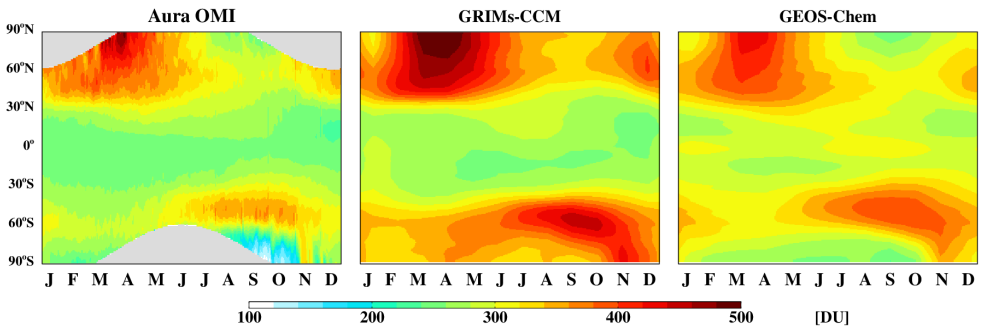

Figure 3.7. The seasonal variation of zonally averaged total column ozone (in Dobson unit) obtained from the **(left)** satellite measurement and simulated from the **(middle)** GRIMs-CCM and **(right)** GEOS-Chem. The model data are integrated from the surface to the model top (0.01 hPa). Gray-shaded indicates the missing data in the Aura-OMI observation.

Compared with the satellite observation and the GEOS-Chem, the GRIMs-CCM shows higher total column ozone in the polar region. **Figure 3.8a** shows the differences in zonally averaged annual mean ozone concentrations between the GRIMs-CCM and the GEOS-Chem. It shows that the ozone differences mainly appear in the stratosphere. The GRIMs-CCM shows higher ozone concentrations at 20–40 km altitude in the polar region and lower ozone concentrations at 20–30 km altitude in the tropics than the GEOS-Chem. **Figures 3.8b** and **3.8c** show the differences in temperature and convective mass fluxes between the two models. The GRIMs-CCM shows lower temperature in the stratosphere, which results in higher ozone concentration than the GEOS-Chem as the local ozone tendency negatively correlates with the temperature, as shown in **Fig. 3.8d**. **Figure 3.8c** shows that the GRIMs-CCM has a stronger convective mass flux in the troposphere. Especially, the stronger convective mass flux near the tropopause can transport the tropospheric air masses into the lower stratosphere, which may lead to a lower ozone concentration in the lower stratosphere.

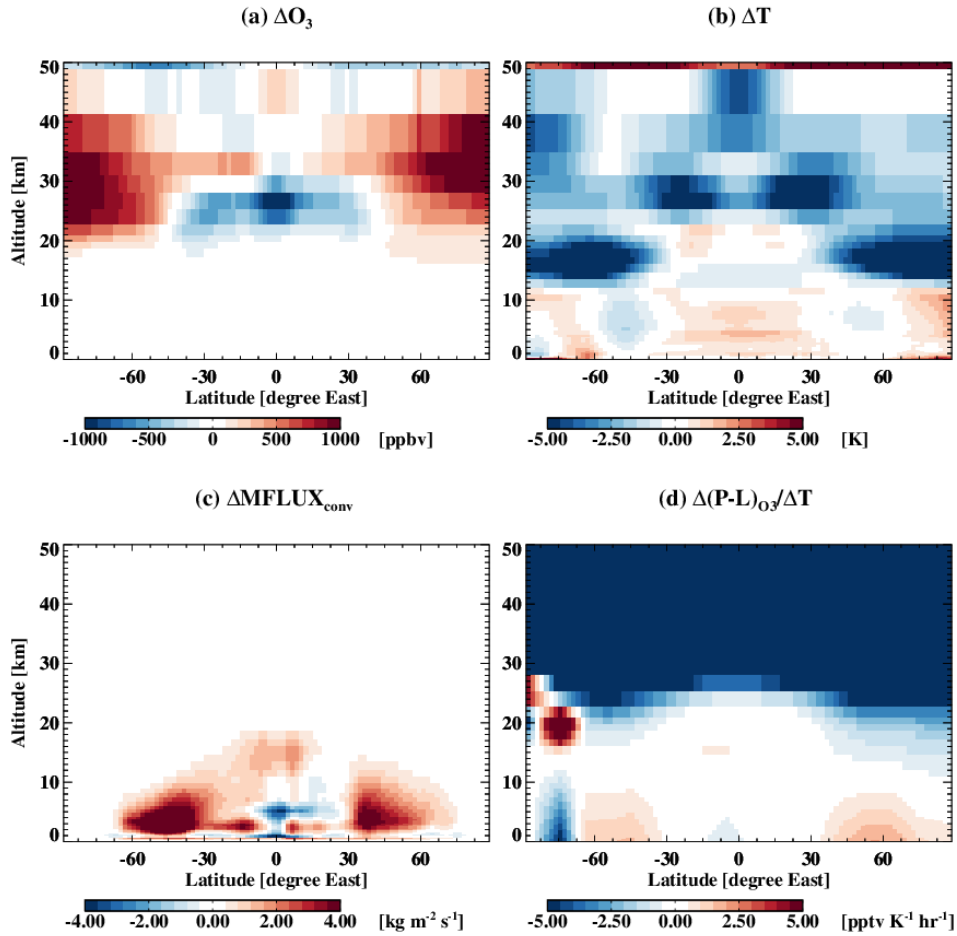

Figure 3.8. The difference (GRIMs-CCM minus GEOS-Chem) of zonally averaged annual mean **(a)** ozone concentration, **(b)** temperature, and **(c)** convective mass flux. **(d)** change of net ozone production in the LINOZ model per local temperature difference from the climatology.

I also compare the tropospheric ozone concentration at different vertical levels using ozonesonde data from the World Ozone and Ultraviolet Radiation Data Centre (WOUDC). The WOUDC sonde data during 2005 is compared with the ozone concentration from the models. The locations of the WOUDC stations where the sonde data are available for 2005 are shown in **Figure 3.9**. **Figure 3.10** shows the seasonal cycle of the tropospheric ozone concentration at 750 hPa, 500 hPa, and 250 hPa altitudes, averaged over 90°S–30°S, 30°S–0°S, 0°N–30°N, and 30°N–90°N latitude bands, respectively. The model data are sampled at the location of the observational data point before averaging. The GRIMs-CCM reproduces the seasonal cycle of tropospheric ozone concentrations except for the 90°S–30°S latitude band at 500hPa, showing high correlation coefficients with the observation (0.50 to 0.97). However, the model underestimates the seasonality of 500-hPa ozone in the Southern Hemisphere high latitudes (90°S–30°S). This bias is related to the strong convective mass flux, resulting in weakening stratospheric ozone influxes in the GRIMs-CCM, as shown in **Fig. 3.8c**. The GEOS-Chem model shows a high correlation coefficient with the observation at all the latitude bands (0.57–0.94) and

generally agrees with the observation, showing the importance of meteorological data for simulating the tropospheric ozone.

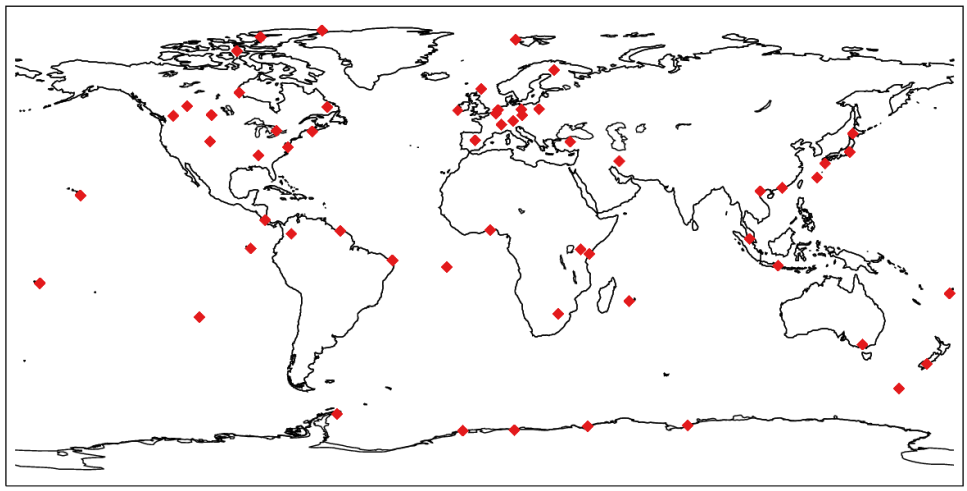

Figure 3.9. The map of locations of WOUDC stations used for the comparison of tropospheric ozone concentration. Red diamonds indicate individual WOUDC stations.

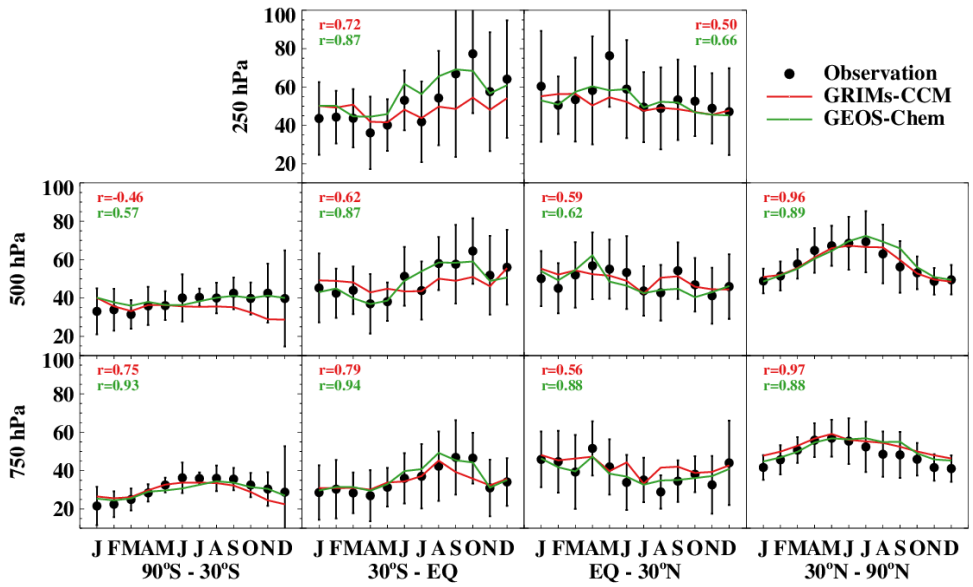

Figure 3.10. Comparison of the seasonal cycle of the tropospheric ozone concentration (in ppbv) at three altitude levels (750 hPa, 500 hPa, 250 hPa) and four latitude bands (90°S–30°S, 30°S–EQ, EQ–30°N, 30°N–90°N) following Stevenson et al. (2006) and Young et al. (2013). The model data are sampled at the location of the WOUDC station before averaging. The filled circles indicate the monthly mean of the observation, and the error bars indicate ±1 standard deviation. The correlation coefficients are shown on the left or right top of the panels.

3.3. Surface Particulate Matter (PM)

I evaluate the simulated PM concentrations with observations from the networks, including the Acid Deposition Monitoring Network in East Asia (EANET), the Interagency Monitoring of Protected Visual Environments (IMPROVE) in the United States, and the European Monitoring and Evaluation Programme (EMEP) in Europe. For East Asia, I use PM_{10} observations for 2005 at 20 EANET sites, measured by automatic monitoring methods, including a β-ray absorption method and a Tapered Element Oscillating Microbalance (TEOM) method. The automatic monitoring data are summed up into monthly data when the data coverage during a given month is more than 50%. The simulated PM_{10} concentrations are calculated as the sum of their constituents' concentrations as follows:

$$PM_{10} = SO_4^{2-} + NO_3^- + NH_4^+ + BC + OC \times 2.1 + Sea\ Salt\ (Accum., Coarse) + Soil\ Dust\ (Bin1 \sim Bin4) \quad (3.1)$$

Figures 3.11a and **3.11b** compare the simulated versus observed annual-mean PM_{10} concentrations in surface air in East Asia. The observed PM_{10} concentrations are high in the continent and are low in the downwind regions, including the Korean peninsula and Japan. Both the GRIMs-CCM and GEOS-Chem reproduce the observed spatial distribution of PM_{10} concentrations with high spatial correlation coefficients (0.83 for GRIMs-CCM and 0.73 for GEOS-Chem). However, the normalized mean biases are negative (−33% for GRIMs-CCM and −18% for GEOS-Chem), indicating that the models underestimate PM_{10} concentrations in East Asia. A larger bias in the GRIMs-CCM compared to the GEOS-Chem partly results from soil dust aerosols from the Gobi Desert. The GRIMs-CCM simulates soil dust aerosols from the Gobi Desert, but their amount is much smaller than GEOS-Chem due to model biases in soil moisture content and surface wind speed.

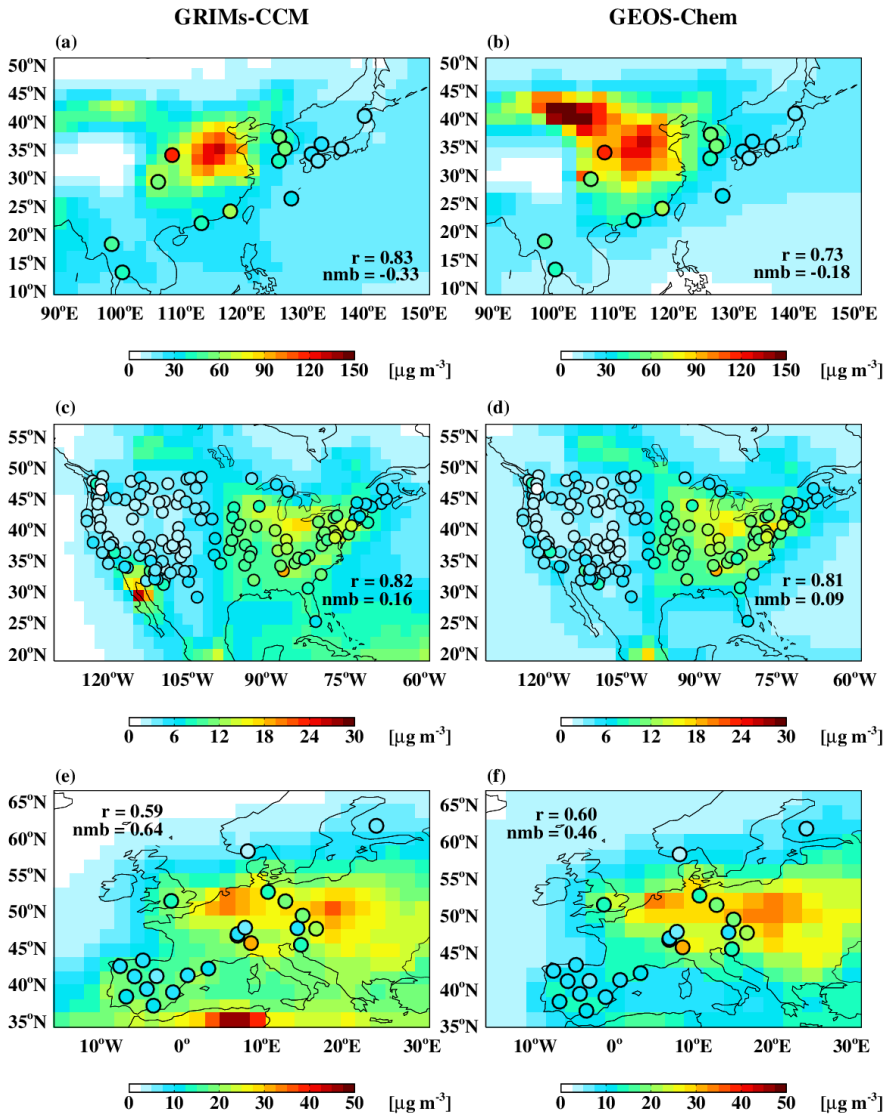

Figure 3.11. Comparison of the spatial distribution of **(a,b)** annual mean PM_{10} mass concentration in East Asia and (c-f) annual mean $PM_{2.5}$ mass concentration in **(c,d)** U.S. and **(e,f)** Europe. The annual mean concentrations at each site (circle) are shown over the annual mean PM_{10} or $PM_{2.5}$ concentrations simulated from the models (shaded).

Figures 3.12a and **3.12b** compare the soil dust emissions in East Asia simulated from the GRIMs-CCM and GEOS-Chem. The GRIMs-CCM simulates much smaller amount of soil dust emissions from the Gobi Desert compared to that of GEOS-Chem. Comparisons of 10m wind speed (**Figs 3.12c** and **3.12d**) and soil moisture content (**Figs 3.12e** and **3.12f**) from the GRIMs-CCM and GEOS-Chem show that the GRIMs-CCM simulates weaker wind speed and higher soil moisture content than the GEOS-Chem in the Gobi Desert, which is unfavorable condition for soil dust emissions.

Figures 3.13a and **3.13b** show scatter plots of the observed versus simulated seasonal mean surface PM_{10} concentrations at EANET sites. Both the GRIMs-CCM and GEOS-Chem capture the observed seasonal variation of surface PM_{10} concentrations in East Asia with high correlation coefficients (0.79 for GRIMs-CCM and 0.67 for GEOS-Chem). However, the regression slope in the GRIMs-CCM is only 0.62 (solid line), again indicating that the model underestimates the observed PM_{10} concentrations. As shown in **Figs. 3.11a** and **3.11b**, lower soil dust emissions from the Gobi Desert in the GRIMs-CCM likely lead to lower PM_{10} concentrations compared to the GEOS-Chem.

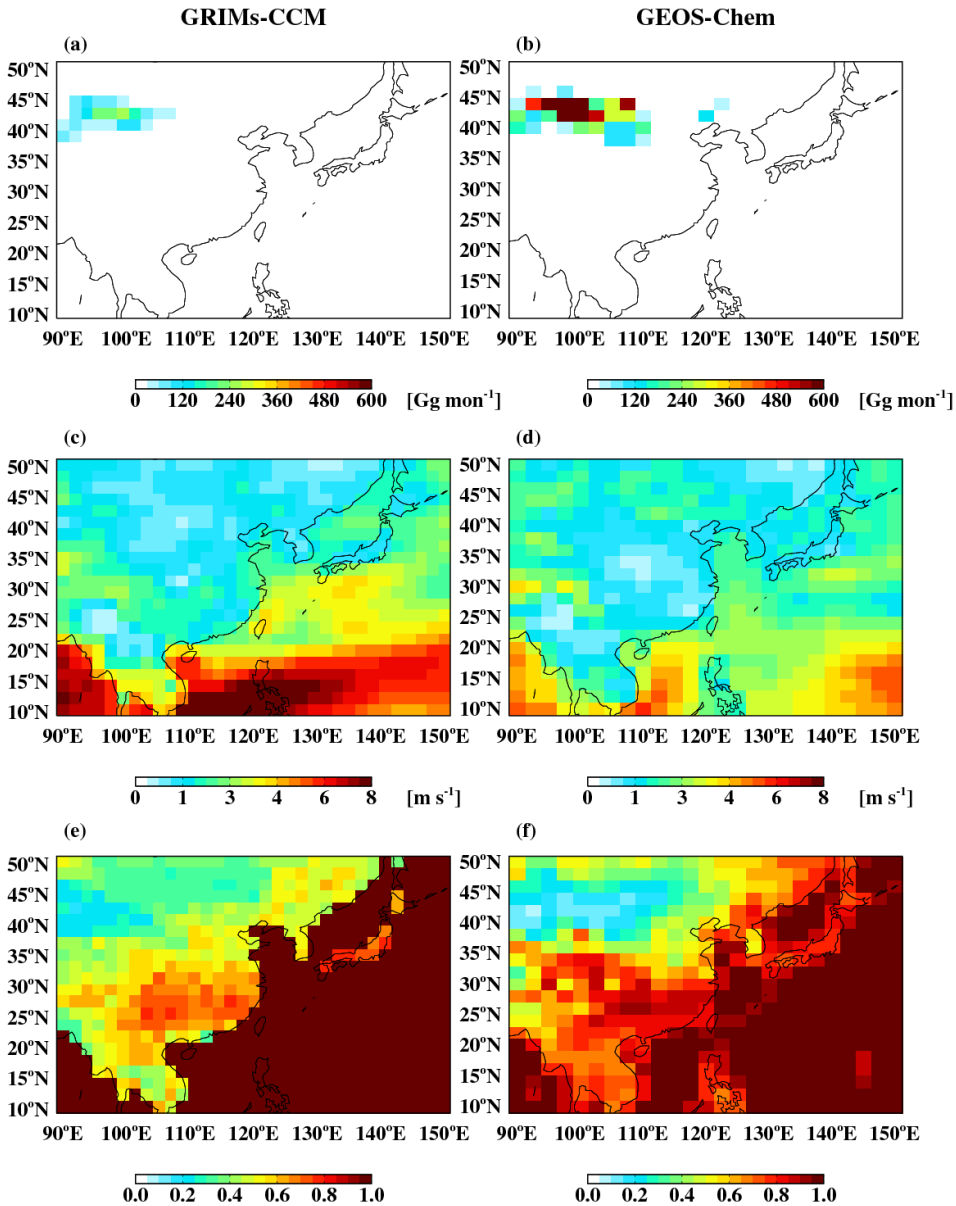

Figure 3.12. Comparison of the simulated spatial distributions of **(a,b)** soil dust emission, **(c,d)** 10m wind speed, and **(e,f)** volumetric soil moisture content in East Asia in spring and summer.

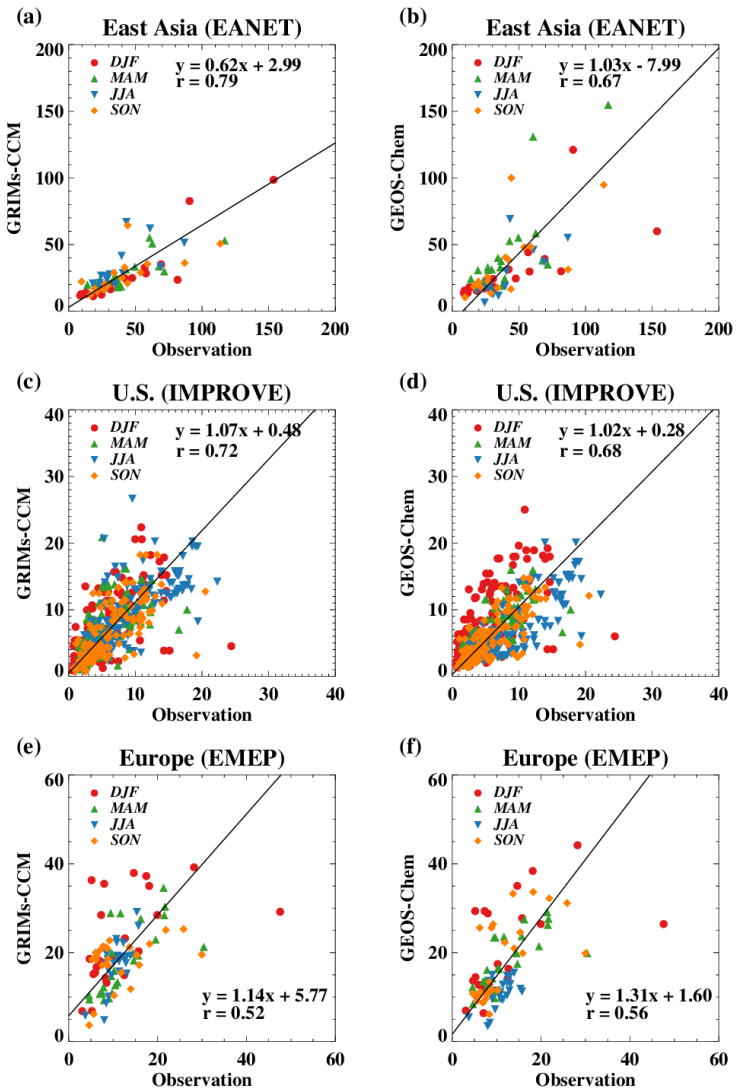

Figure 3.13. Scatter plots of seasonal mean **(a,b)** PM_{10} concentrations at each EANET site and (c-f) $PM_{2.5}$ concentrations at **(c,d)** IMPROVE and **(e,f)** EMEP sites. The unit is in μg m^{-3}. Each point indicates the seasonal mean PM_{10} or $PM_{2.5}$ concentration at each observation site. The regression slope is calculated using the reduced major axis method.

For the United States, I use the $PM_{2.5}$ observations for 2005 at 178 IMPROVE sites (**Figs. 3.11c** and **3.11d**). Notice that $PM_{2.5}$ instead of PM_{10} observations are used here. The daily $PM_{2.5}$ concentrations at IMPROVE sites are measured by weighing the 25-mm Teflon filter before and after sampling every three days using a microbalance (Malm et al., 1994). The simulated $PM_{2.5}$ concentrations are calculated similarly to PM_{10}, but the coarse mode sea salt aerosols and soil dust bin 2 to 4 are excluded.

Figures 3.11c and **3.11d** show comparisons of annual-mean surface $PM_{2.5}$ concentrations between the models and the observations in the United States. The observed $PM_{2.5}$ concentrations are high in the eastern United States and are low in the western United States. Both models reasonably reproduce the observed spatial distribution with high spatial correlation coefficients (0.82 for GRIMs-CCM and 0.81 for GEOS-Chem) and slight overestimations (+16% bias in GRIMs-CCM and +9% bias in GEOS-Chem). The GRIMs-CCM shows high $PM_{2.5}$ concentrations over the Baja California Peninsula. High concentrations of soil dust aerosols from the Sonoran Desert are simulated from late spring to summer in the GRIMs-CCM. In this season, the high concentrations of dust aerosols affect a large area of

Southwestern US in GRIMs-CCM, while the observation and the GEOS-Chem do not show the increase of PM due to dust aerosols.

Figures 3.13c and **3.13d** show scatter plots of the observed versus simulated seasonal-mean surface $PM_{2.5}$ concentrations at IMPROVE sites. Both the GRIMs-CCM and GEOS-Chem reproduce the observed seasonal variation of surface $PM_{2.5}$ concentrations with high correlation coefficients (0.72 for GRIMs-CCM and 0.68 for GEOS-Chem) and regression slopes close to unity (1.07 for GRIMs-CCM and 1.02 for GEOS-Chem). However, both models show higher concentrations of $PM_{2.5}$ in December–January–February (DJF) (37% bias in GRIMs-CCM and 58% in GEOS-Chem).

Figures 3.11e and **3.11f** compare the simulated versus observed annual-mean surface $PM_{2.5}$ concentrations at EMEP sites in Europe. The $PM_{2.5}$ observation data are available at 25 EMEP sites from 11 countries in 2005. In most sites, $PM_{2.5}$ concentrations are measured by the gravimetric method using high or low volume samplers. An exception is those from Sweden, where the automatic TEOM method is used. The observation shows relatively high $PM_{2.5}$ concentrations in central Europe and low concentrations in the Iberian and the Scandinavian Peninsula. The simulated

$PM_{2.5}$ concentrations from both models show very similar spatial distribution with a spatial correlation of 0.6. However, both models simulate higher $PM_{2.5}$ concentrations in central Europe, including Germany and the Czech Republic, than the observation. The normalized mean biases are 64% for GRIMs-CCM and 46% for GEOS-Chem. High concentrations of soil dust aerosols in northern Africa simulated in GRIMs-CCM but not in GEOS-Chem, contribute to the higher bias in GRIMs-CCM.

Figures 3.13e and **3.13f** show scatter plots of the observed versus simulated seasonal mean surface $PM_{2.5}$ concentrations. The models appear to capture the observed seasonal variation of $PM_{2.5}$ concentration in Europe with correlation coefficients of 0.52 for GRIMs-CCM and 0.56 for GEOS-Chem. The positive bias of simulated $PM_{2.5}$ concentrations against the observation is the highest in DJF when the normalized mean biases are 89% for GRIMs-CCM and 75% for GEOS-Chem. This bias is mainly due to inorganic nitrate aerosol, often overestimated by several atmospheric chemistry models (Bian et al., 2017; Tuccella et al., 2012; Walker et al., 2012; Zhang et al., 2012).

4. Aerosol Radiative Forcing

The aerosol radiative forcing (RF) is an effective indicator of the impact of aerosols on climate change (Forster et al., 2007; Intergovernmental Panel on Climate Change, 2013; Myhre et al., 2013; Shindell et al., 2013). The aerosol RF is the imbalance of net radiative flux at the tropopause due to aerosol changes. I estimate the direct aerosol RF due to aerosol changes from the preindustrial era to the present day using 10-year time-slice GRIMs-CCM simulations. Two sets of 10-year model simulations starting from 1850 (preindustrial) and 2000 (present-day) are conducted with the default setting as described in section 3. For each simulation, the SST, sea-ice concentrations from 1850 to 1859 and from 2000 to 2009 are prescribed. I also consider the temporal change of greenhouse gases by prescribing global mean concentrations of CO_2, CH_4, N_2O, and CFCs from Meinshausen et al. (2011). The default emission databases in the GRIMs-CCM package described in section 2.2 do not cover the preindustrial era. Thus, I use the emission inventory for ACCMIP (Lamarque et al., 2010), which covers 1850 to 2000, for the anthropogenic

and biomass burning emissions. The ACCMIP emission inventory has a time resolution of a decade, so I use the data for 1850 to simulate 1850–1859 and the data for 2000 to simulate 2000–2009. I calculate the radiative flux change due to aerosols by conducting a pair of radiative transfer calculations with and without aerosols for each simulation, and the difference in the flux change at the top of the atmosphere (TOA) due to the aerosols between the two simulations is defined as direct aerosol RF.

Figure 4.1 shows the simulated aerosol direct RF due to aerosol changes from the preindustrial to the present climate. The simulated global mean aerosol direct RF is −0.30 W m^{-2}. Values are spatially uneven, showing strong negative RF in East Asia and Europe. **Figures 4.2a**–**4.2c** show that the amount of anthropogenic sulfate-nitrate-ammonium is significantly increased in East Asia and Europe, which explains the strong negative aerosol RF in East Asia and Europe. The sulfate-ammonium-nitrate aerosols are also increased in the US, but OC aerosols are decreased in this region, which cancels out the effect of increased sulfate-nitrate-ammonium aerosols. The negative RF is also shown in central Africa due to increased BC and OC aerosols (**Figs. 4.2b** and **4.2c**) from increased biomass burning

emission in the present day (Lamarque et al., 2010) and in western tropical Africa due to increased soil dust aerosols (**Fig. 4.2d**).

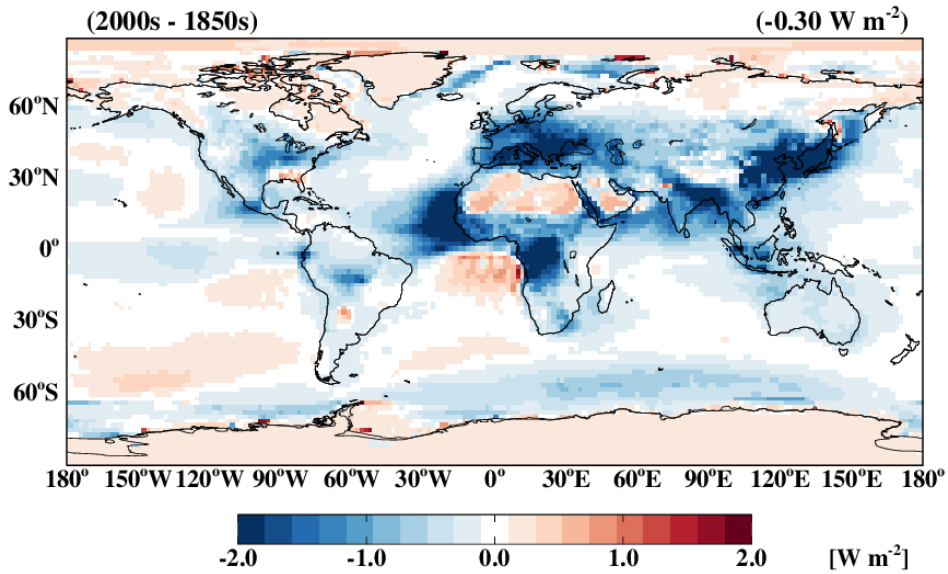

Figure 4.1. Preindustrial to present-day aerosol RF calculated using GRIMs-CCM 10-year time-slice simulations for the 1850s and 2000s. The mean aerosol RF is indicated in the parenthesis in the upper right corner.

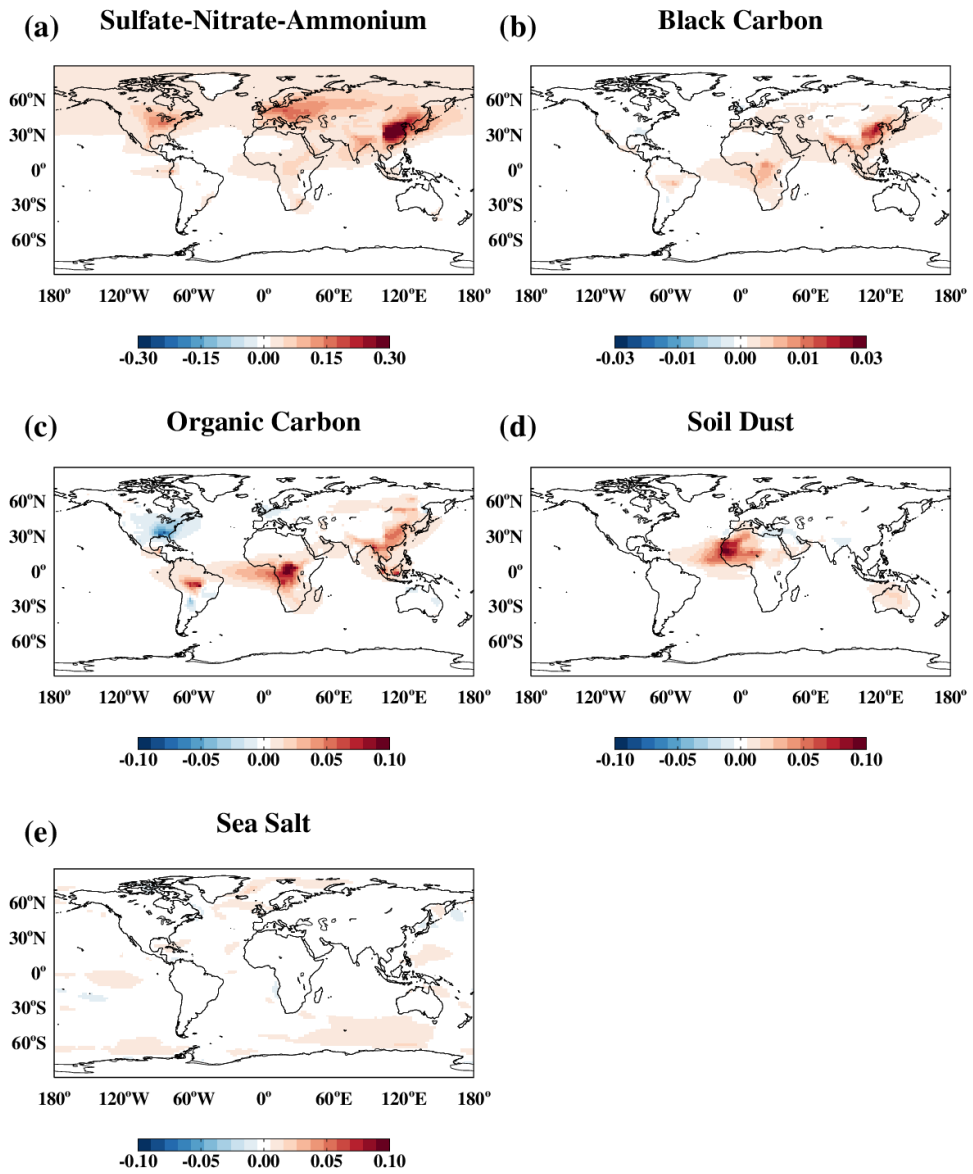

Figure 4.2. Preindustrial to present-day AOD change by **(a)** sulfate-nitrate-ammonium aerosols, **(b)** black carbon, **(c)** organic carbon, **(d)** soil dust aerosols, and **(e)** sea salt aerosols.

Figure 4.3 compares the global mean aerosol direct RF with the aerosol direct RF from the ACCMIP models in Shindell et al. (2013) and AEROCOM Phase II models in Myhre et al. (2013). The aerosol direct RFs from the models participating in the ACCMIP and AEROCOM Phase II are calculated in the same way as in this study (the flux change at TOA for simulation with present and preindustrial emissions). The mean aerosol direct RF from 10 ACCMIP models is −0.26 W m^{-2} (stddev of 0.14). Likewise, the mean aerosol direct RF from 16 AEROCOM Phase II models is −0.27 W m^{-2} (stddev of 0.15). The global mean aerosol direct RF calculated from the GRIMs-CCM simulations (−0.30 W m^{-2}) is close to the mean values from ACCMIP and AEROCOM Phase II. This result indicates that the GRIMs-CCM estimates the aerosol RF as a comparable level to the other climate models.

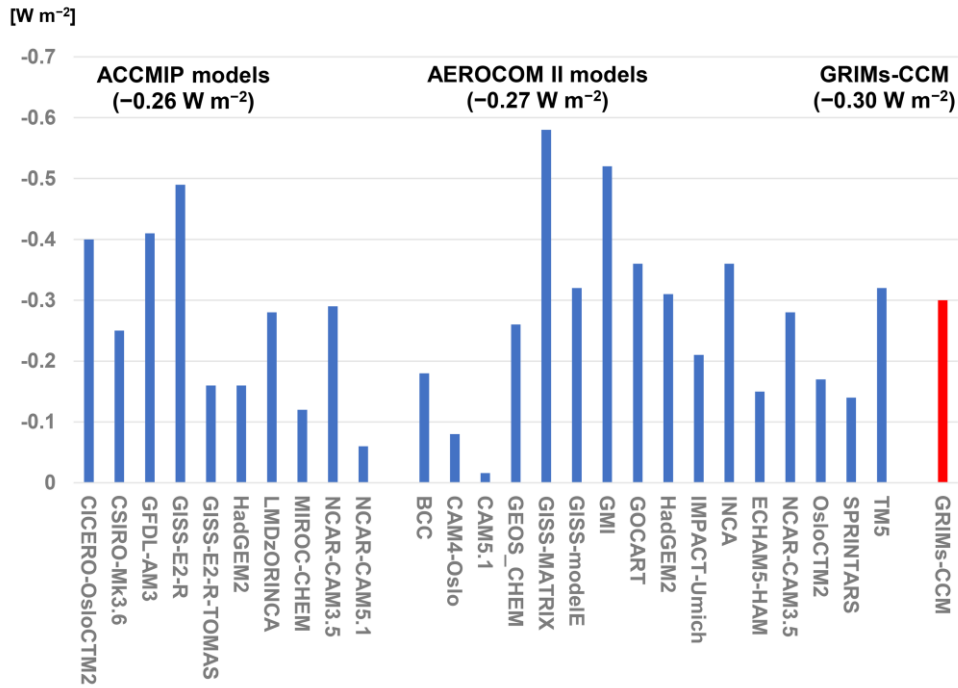

Figure 4.3. Comparison of global mean preindustrial to present-day aerosol radiative forcing from the GRIMs-CCM, ACCMIP models, and AEROCOM II models.

5. Effects of Aerosol Changes on Regional Climate

5.1 Recent Aerosol Changes in East Asia

East Asia has become the largest emitter of aerosols, and their precursors since the anthropogenic emissions of air pollutants in East Asia were continuously increased after 1950 (Smith et al., 2011). The surface measurement of $PM_{2.5}$ concentrations and the retrieval of aerosol optical depth from the satellite show that a large amount of aerosols exists in East Asia (Ding et al., 2019; Shindell et al., 2013). The dominant aerosol species in East Asia are anthropogenic inorganic aerosols such as sulfate, nitrate, ammonium, and carbonaceous aerosols. The last includes black carbon, primary organic carbon, and secondary organic carbon (Myhre et al., 2013; Shindell et al., 2013). They interact with the climate system by effectively scattering or absorbing the solar radiation, which results in strong negative radiative forcings, as shown in section 4.

The high concentrations of $PM_{2.5}$ in China have become an environmental issue as the tiny aerosol particles smaller than 2.5 microns in

diameter are known to be harmful to human health and negatively affect the visibility (Cao et al., 2012; Malm et al., 2004; Zhang et al., 2017). To alleviate particulate air pollution, the Chinese government commenced a strict emission control plan named Air Pollution Prevention and Control Action Plan in 2013 (Liu et al., 2019; Liu et al., 2018; Sheehan et al., 2014; Wang et al., 2017; Zheng et al., 2018). Zheng et al. (2018) estimated that the anthropogenic emission in China decreased by 59% for SO_2, 21% for NO_X, 23% for CO, 36% for PM_{10}, 33% for $PM_{2.5}$, 28% for BC, and 32% for OC during 2013–2017. Surface measurements of $PM_{2.5}$ in China reveal that the emission control by the government is effective, showing evidence of decreased $PM_{2.5}$ concentrations. Long-term measurement of $PM_{2.5}$ and its chemical components at a station in eastern China, the Station for Observing Regional Processes of the Earth System (SORPES), shows that the concentrations of $PM_{2.5}$, BC, and sulfate aerosol at the station are decreased by 9.1%, 8.4%, and 10.6% respectively from 2013 to 2018 (Ding et al., 2019).

Air pollution reduction in East Asia is also clearly shown in the satellite measurement of aerosol optical depth. **Figure 5.1** shows the

timeseries of aerosol optical depth from the MODIS averaged in East Asia in November-December-January-February-March-April (NDJFMA) season. The aerosol optical depth in East Asia continuously increased from 2001 to 2007 (P1 period), whereas it significantly decreased from 2011 to 2017 (P2 period). **Figures 5.2a** and **5.2b** show spatial map of linear trends of NDJFMA aerosol optical depth in East Asia for the P1 and P2 periods. The positive linear trends shown in the P1 period are changed to negative trends in the P2 period. The decrease of aerosol optical depth mainly appears in China. The mean aerosol optical depth in East Asia decreased by more than 25% in the P2 period.

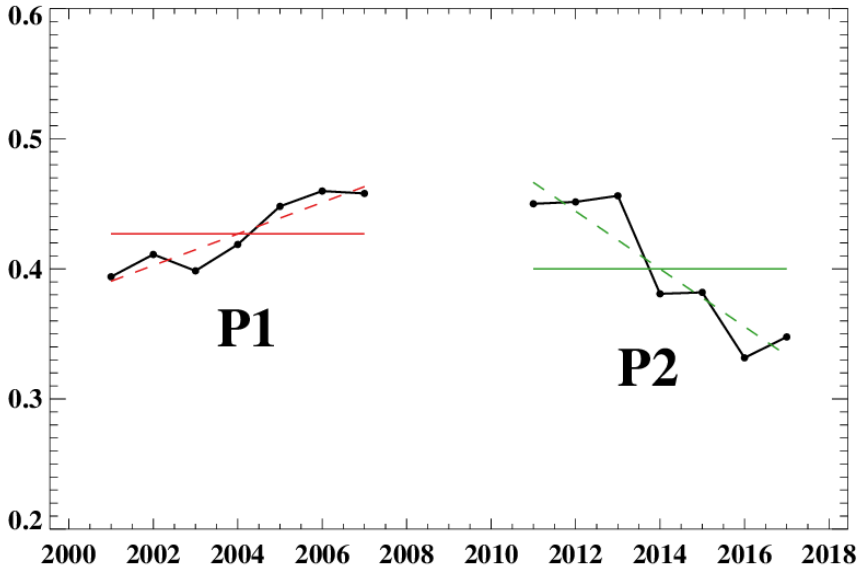

Figure 5.1. Linear trends of aerosol optical depth at 550 nm in East Asia observed from MODIS in November–December–January–February–March–April season during 2001–2017. P1 indicates the increasing aerosol period from 2001 to 2007, whereas P2 indicates the decreasing aerosol period from 2011 to 2017.

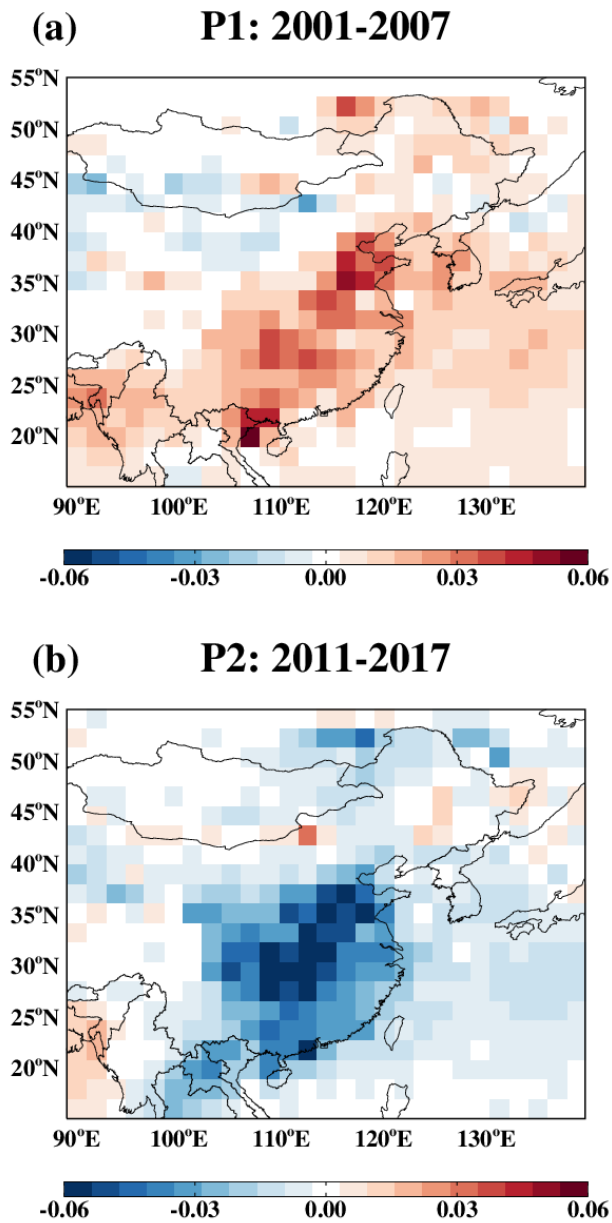

Figure 5.2. 2-D map of linear trends of aerosol optical depth from MODIS in East Asia during **(a)** 2001–2007 (P1 period) and **(b)** 2011–2017 (P2 period).

As the aerosols effectively scatter or absorb the solar radiation, the aerosols change in East Asia should impact the regional climate. Along with the decrease of aerosol loadings, positive trends in 2-m air temperature are shown in East Asia. **Figure 5.3** shows linear trends of 2-m temperature in East Asia in the NDFJMA season during 2011–2017 calculated using ERA-Interim reanalysis data. The positive temperature trends mainly appear in China, consistent with the change of aerosol optical depth shown in **Figure 5.2b**. I try to explain the relationship between the aerosol and temperature changes shown in the reanalysis data by conducting climate simulations using GRIMs-CCM and Community Earth System Model (CESM).

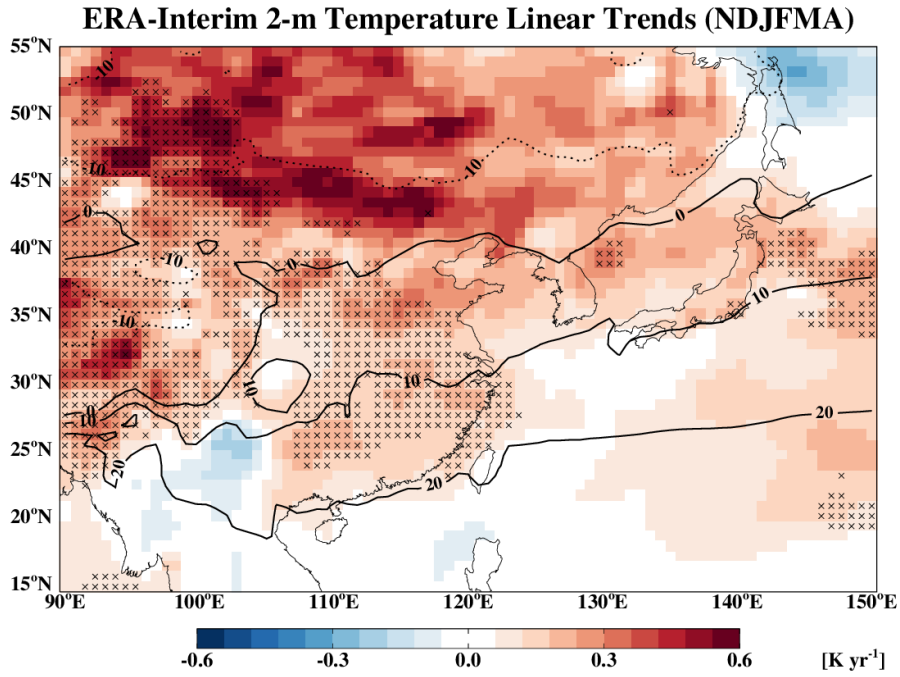

Figure 5.3. 2-D map of linear trends of 2-m temperature averaged in NDJFMA season from ERA-Interim reanalysis dataset. The contours indicate climatological mean temperature, and the shades indicate linear trends. Cross marks denote the grid-point where the linear trend is different from zero at the 90% confidence level based on the student's t-test.

5.2 Experiment Setup

I conducted two sets of climate sensitivity simulations (Base run and Sensitivity run) using GRIMs-CCM and CESM from 2011 to 2017 when the decrease of aerosol optical depth is shown in the measurements. The aerosol optical properties, including aerosol optical depth, single scattering albedo, and asymmetry parameters for the simulations, are prescribed with monthly data from the 1-year GRIMs-CCM simulation. For the Base run, the aerosol optical depth prescribed in the model is scaled to monthly MODIS aerosol optical depth from 2011 to 2017 to reflect the temporal change of aerosol optical depth, while the monthly averaged aerosol optical depth is prescribed for the sensitivity run. The NCEP-DOE AMIP-II Reanalysis (R-2) data (Kanamitsu et al., 2002) are used for the initial condition, and the Global sea-Ice and SST (GISST) data (Rayner et al., 1996) are prescribed for the sea surface temperature (SST) and sea-ice concentration for both GRIMs-CCM and CESM. For the CO_2 concentration, a global mean value of 379 ppm is applied to the GRIMs-CCM, and a global mean value of 367 ppm is used to the CESM. The GRIMs-CCM model has a T62 horizontal

grid resolution, which corresponds to about 200 km grid space in the equator, and 47 vertical layers. The CESM model has 2.5°x1.9° (longitude, latitude) horizontal resolution and 26 vertical layers. Each simulation set consists of 20 ensemble members with slightly different initial conditions to minimize the effect of internal model variability. I analyze the climatic impact of aerosol changes by comparing the Base run and Sensitivity run.

5.3 Results and Discussions

First, I evaluated the models' performance of reproducing the temperature warming in East Asia during 2011–2017. **Figures 5.4a** and **5.5a** show linear surface temperature trends from the Base run of GRIMs-CCM (**Fig. 5.4a**) and CESM (**Fig. 5.5a**). The models couldn't capture the strong warming signal in the high latitudes shown in ERA-Interim reanalysis data (**Fig. 5.3**). Still, both models successfully capture the warming trend of surface temperature in East Asia, especially over the aerosol source region. **Figures 5.4b** and **5.5b** show linear surface temperature trends from the Sensitivity run of GRIMs-CCM (**Fig. 5.4b**) and CESM (**Fig. 5.5b**). The results of the Sensitivity run also show the warming trend of surface temperatures in East Asia. Still, the magnitude is weaker than the Base run result, which means that the decrease of aerosols during 2011–2017 contributes to the warming of temperature in East Asia. **Figure 5.6** shows the difference in temperature trends between the Base run and the Sensitivity run (Base run minus Sensitivity run), which means the climatic effect of aerosol change on the temperature change in East Asia during

2011–2017. Both GRIMs-CCM and CESM models show consistent results, indicating the positive temperature trends due to the reduction of aerosols in East Asia. The mean temperature increase in the region where the box indicates in **Figure 5.6** (105°E–120°E, 22°N–30°N) is 0.053 K $year^{-1}$ for GRIMs-CCM and 0.074 K $year^{-1}$ for CESM.

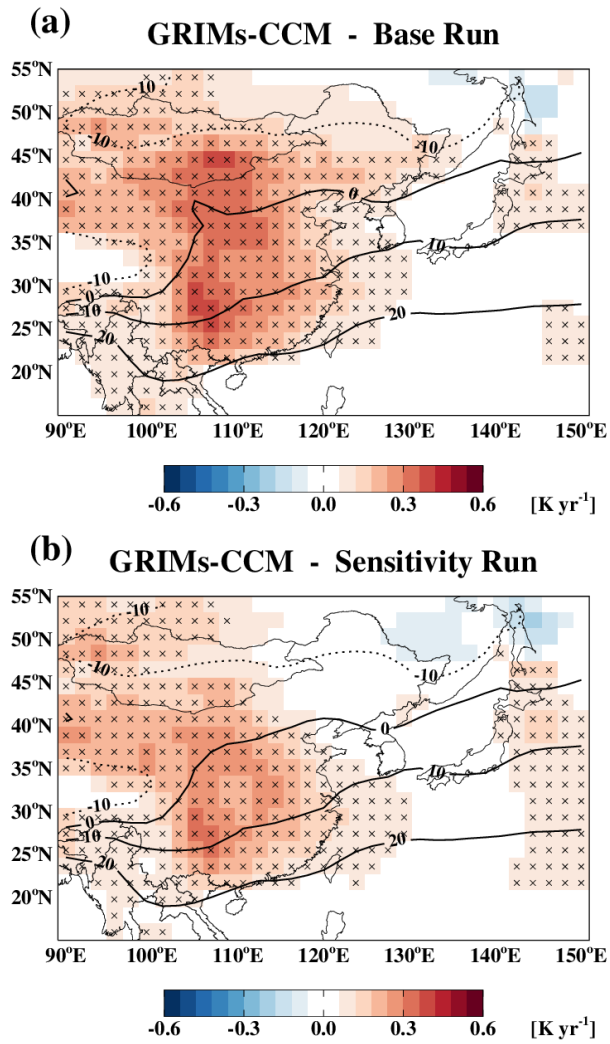

Figure 5.4. 2-D map of linear trends of 2-m temperature averaged in NDJFMA season from GRIMs-CCM **(a)** Base run and **(b)** Sensitivity run. The contours indicate climatological mean temperature, and the shades indicate linear trends. Cross marks denote the grid-point where the linear trend is different from zero at the 90% confidence level based on the student's t-test.

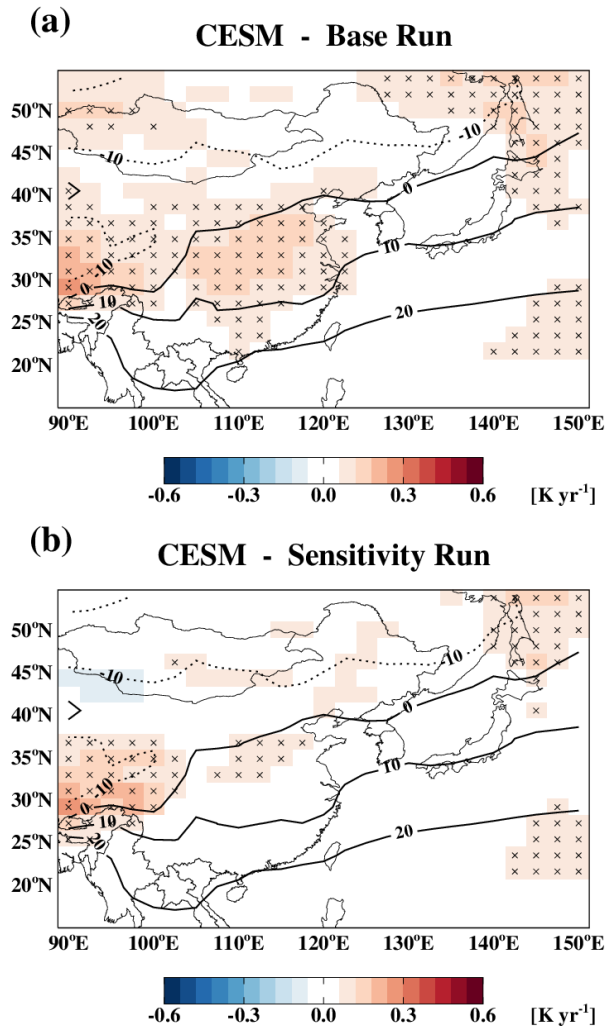

Figure 5.5. Same as **Figure 5.4**, but the data from CESM **(a)** Base run and **(b)** Sensitivity run.

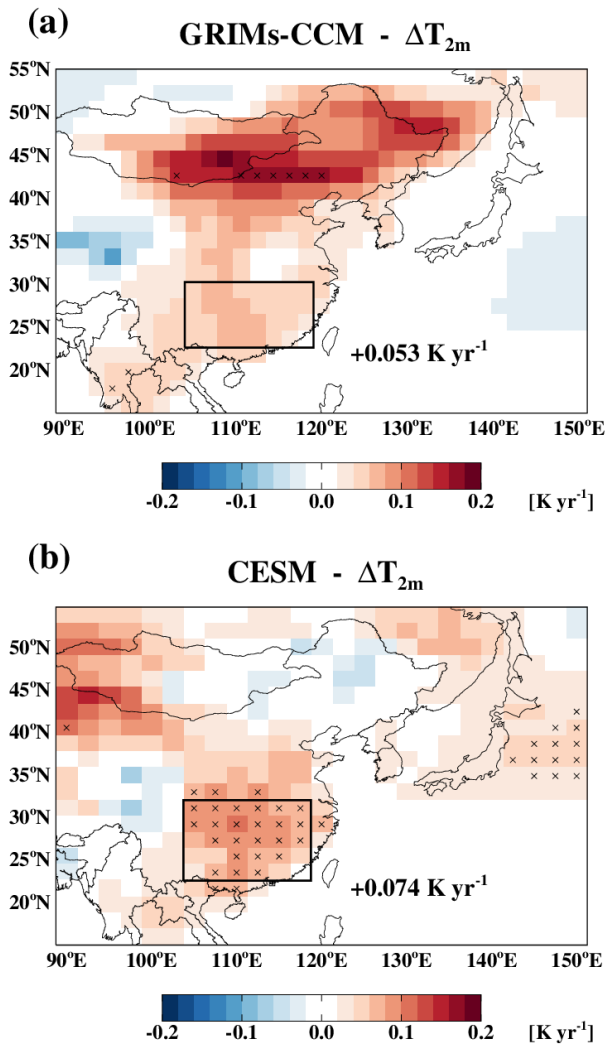

Figure 5.6. 2-D map of difference of 2-m temperature trends between Base run and Sensitivity run (Base run minus Sensitivity run) averaged in NDJFMA season for **(a)** GRIMs-CCM and **(b)** CESM. Cross marks denote the grid-point where the linear trends of the two models are different at the 90% confidence level based on the student's t-test.

Figure 5.7 shows the differences in trends of various meteorological variables between the Base run and the Sensitivity run from GRIMs-CCM and CESM. The differences between the Base run and the Sensitivity run imply the effects of aerosol reduction on the meteorological variables. **Figures 5.7a** and **5.7b** show the changes in downward solar radiation at the surface from GRIMs-CCM and CESM. Both models show consistent results of increased solar radiation due to decreased aerosols that scatter the solar radiation. The CESM shows a stronger increase of solar radiation than the GRIMs-CCM, which is the main reason for the more substantial temperature increase shown in **Figure 5.6**. **Figures 5.7c** and **5.7d** show the change in precipitation from GRIMs-CCM and CESM. Both models consistently show a decreased rainfall in in southern China, where downward solar radiation and temperature have positive trends. **Figures 5.7e** and **5.7f** show the planetary boundary layer height change from GRIMs-CCM and CESM. The planetary boundary layer heights are consistently showing positive trends in both models. The increased solar radiation due to aerosol reduction provides more energy to the surface and active turbulent mixing, which increases planetary boundary layer height.

The high planetary boundary layer may help improve surface air quality by diluting and ventilating pollutants within the planetary boundary layer.

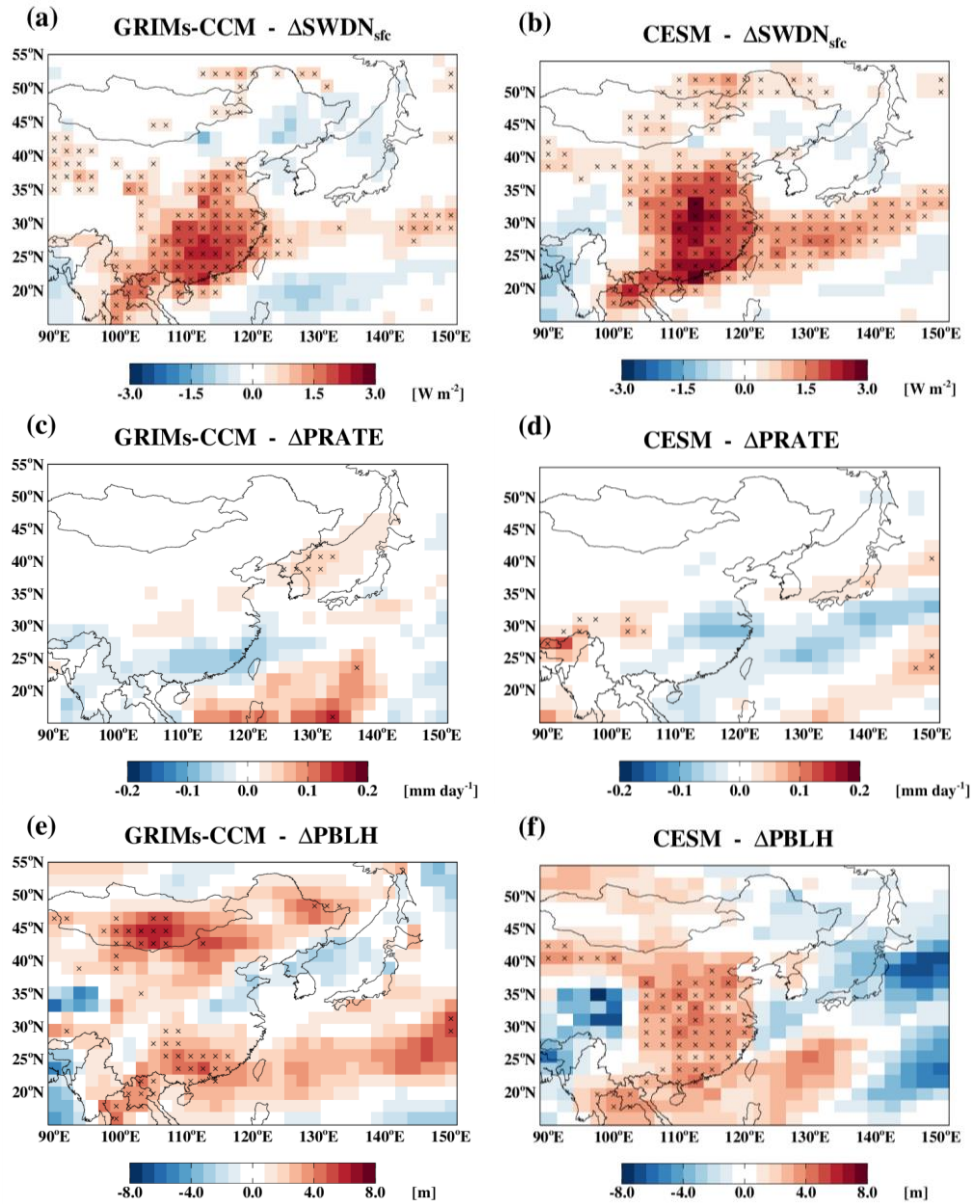

Figure 5.7. Same as **Figure 5.6** but for the various meteorological variables. **(a,b)** for downward solar radiation at the surface (units are W m^{-2}), **(c,d)** for precipitation (units are mm day^{-1}), and **(e,f)** for planetary boundary layer height (units are m).

6. Summary and Conclusions

The SLCPs are considered the essential components for future climate projection because of the high uncertainty of their climatic impacts. The chemistry-climate model is much needed to better understand the chemistry-climate interaction. In this regard, I developed a new chemistry-climate model by coupling the GEOS-Chem's chemistry modules into the GRIMs, GRIMs-CCM. I describe each component of the model and conduct the model evaluation to assess the new model's performance by focusing on ozone, aerosols, and aerosol radiative forcing.

I first conducted a 1-year simulation for 2005. Comparing GRIMs-CCM AOD with the satellite retrieved AOD reveals that the model captures the spatial distribution of annual-mean AOD but underestimates its magnitude by −19%. The budget analyses for the aerosols show that removing aerosols from the atmosphere is faster in the GRIMs-CCM than in the reference model, GEOS-Chem, due to more vigorous cumulus convection and surface friction velocity.

The model adequately reproduces the seasonal and latitudinal variation of total column ozone. However, it exhibits a significant bias in the polar stratospheric ozone due to a cold bias of stratospheric temperature. The comparison also reveals that the model has difficulty reproducing the Antarctic ozone hole due to ignorance of complex halogen chemistry. It tells us that the future version of the GRIMs-CCM should consider the halogen species with heterogeneous chemistry to better represent the stratospheric ozone. It is further found that the model can simulate the seasonal variation of tropospheric ozone. However, the GEOS-Chem model with the assimilated meteorological fields shows generally better agreement with the observations than the GRIMs-CCM, indicating the importance of meteorological data for simulating tropospheric ozone.

The comparisons of the simulated surface PM with the in-situ measurements in East Asia, the United States, and Europe show that the GRIMs-CCM can reproduce surface PM's temporal and spatial variations with high correlation coefficients (0.79 for East Asia, 0.72 for the US, 0.52 for Europe). However, the GRIMs-CCM has difficulties in simulating soil dust aerosols showing different spatial patterns from the GEOS-Chem. The

underestimation of soil dust in the Gobi Desert and drastic dust emission in northern Africa result in a low bias in East Asia and a high bias in Europe.

The aerosol radiative forcing is estimated to measure the overall climatic influence of aerosols. The preindustrial to present-day global-mean aerosol radiative forcing is −0.30 W m^{-2}. This value is comparable to the aerosol radiative forcing in other climate model comparison projects (−0.26 W m^{-2} for ACCMIP models, −0.27 W m^{-2} for AEROCOM II models).

I finally investigate the regional climatic impact of aerosols in East Asia by conducting sensitivity analyses using GRIMs-CCM and CESM. I conduct 20 ensembles of 7-year simulations prescribing a recently decreasing trend of aerosol optical depth in East Asia observed from the satellite measurements to the models. It is found that the ensemble means of GRIMs-CCM and CESM reproduce positive trends of recent wintertime surface temperature in East Asia shown in the ERA-Interim reanalysis data. I also conduct sensitivity simulations prescribing monthly mean aerosol optical depth without annual trends. Comparisons of model results with and without aerosol optical depth trends show that the models with decreasing aerosol optical depth simulate stronger warming trends in surface

temperature. It indicates that the recent reduction of aerosols in East Asia partly contributes to the positive trends in surface temperature in East Asia.

Our results suggest that the GRIMs-CCM successfully simulates the chemical processes in the atmosphere and aerosol radiative forcing but also reveal that the model has several issues to be addressed in a future study. The update of physics schemes for the underlying atmospheric model may significantly contribute to improving chemistry simulation. Specifically, the update of the land surface model could contribute to the better simulation of soil dust aerosol, which is highly dependent on the surface soil moisture content and surface wind speed. The improvement of ozone simulation could also be fulfilled by resolving the cold temperature bias problem in the stratosphere. Shortly, the GRIMs-CCM will be further improved with the updates in the atmospheric model (Koo et al., 2022) and GEOS-Chem.

Bibliography

Alexander, B., Park, R. J., Jacob, D. J., Li, Q. B., Yantosca, R. M., Savarino, J., Lee, C. C. W., and Thiemens, M. H.: Sulfate formation in sea-salt aerosols: Constraints from oxygen isotopes, Journal of Geophysical Research-Atmospheres, 110 (2005). https://doi.org/10.1029/2004jd005659

Balis, D., Koukouli, M. E., Brinksma, E. J., Kroon, M., Veefkind,J. P., Labow, G., and McPeters, R. D.: Validation of Ozone Monitoring Instrument total ozone column measurements using Brewer and Dobson spectrophotometer ground-based observations, Journal of Geophysical Research-Atmospheres, 112 (2007). https://doi.org/10.1029/2007jd008796

Bey, I., Jacob, D. J., Yantosca, R. M., Logan, J. A., Field, B. D., Fiore, A. M., Li, Q. B., Liu, H. G. Y., Mickley, L. J., and Schultz, M. G.: Global modeling of tropospheric chemistry with assimilated meteorology: Model description and evaluation, Journal of Geophysical Research-

Atmospheres, 106, 23073-23095 (2001).
https://doi.org/10.1029/2001jd000807

Bian, H. S., Chin, M., Hauglustaine, D. A., Schulz, M., Myhre, G., Bauer, S. E., Lund, M. T., Karydis, V. A., Kucsera, T. L., Pan, X. H., Pozzer, A., Skeie, R. B., Steenrod, S. D., Sudo, K., Tsigaridis, K., Tsimpidi, A. P., and Tsyro, S. G.: Investigation of global particulate nitrate from the AeroCom phase III experiment, Atmospheric Chemistry and Physics, 17, 12911-12940 (2017).
https://doi.org/10.5194/acp-17-12911-2017

Bond, T. C., Bhardwaj, E., Dong, R., Jogani, R., Jung, S. K., Roden, C., Streets, D. G., and Trautmann, N. M.: Historical emissions of black and organic carbon aerosol from energy-related combustion, 1850-2000, Global Biogeochemical Cycles, 21 (2007).
https://doi.org/10.1029/2006gb002840

Cao, J., Xu, H., Xu, Q., Chen, B., and Kan, H.: Fine Particulate Matter Constituents and Cardiopulmonary Mortality in a Heavily Polluted Chinese City, Environmental Health Perspectives, 120, 373-378

(2012).
https://doi.org/doi:10.1289/ehp.1103671

Chang, E. C., Yeh, S. W., Hong, S. Y., and Wu, R. G.: Sensitivity of summer precipitation to tropical sea surface temperatures over East Asia in the GRIMs GMP, Geophysical Research Letters, 40, 1824-1831 (2013). https://doi.org/10.1002/grl.50389

Charlson, R. J., Schwartz, S. E., Hales, J. M., Cess, R. D., Coakley, J. A., Jr., Hansen, J. E., and Hofmann, D. J.: Climate forcing by anthropogenic aerosols, Science, 255, 423-430 (1992). https://doi.org/10.1126/science.255.5043.423

Chin, M., Ginoux, P., Kinne, S., Torres, O., Holben, B. N., Duncan, B. N., Martin, R. V., Logan, J. A., Higurashi, A., and Nakajima, T.: Tropospheric aerosol optical thickness from the GOCART model and comparisons with satellite and Sun photometer measurements, Journal of the atmospheric sciences, 59, 461-483 (2002). https://doi.org/10.1175/1520-0469(2002)059<0461:Taotft>2.0.Co;2

Clough, S. A., Shephard, M. W., Mlawer, E., Delamere, J. S., Iacono, M.,

Cady-Pereira, K., Boukabara, S., and Brown, P. D.: Atmospheric radiative transfer modeling: a summary of the AER codes, Journal of Quantitative Spectroscopy & Radiative Transfer, 91, 233-244(2005). https://doi.org/10.1016/j.jqsrt.2004.05.058

Damian, V., Sandu, A., Damian, M., Potra, F., and Carmichael, G. R.: The kinetic preprocessor KPP - a software environment for solving chemical kinetics, Computers & Chemical Engineering, 26, 1567-1579 (2002). https://doi.org/10.1016/S0098-1354(02)00128-X

Ding, A., Huang, X., Nie, W., Chi, X., Xu, Z., Zheng, L., Xu, Z., Xie, Y., Qi, X., Shen, Y., Sun, P., Wang, J., Wang, L., Sun, J., Yang, X. Q., Qin, W., Zhang, X., Cheng, W., Liu, W., Pan, L., and Fu, C.: Significant reduction of PM2.5 in eastern China due to regional-scale emission control: evidence from SORPES in 2011-2018, Atmos. Chem. Phys., 19, 11791-11801 (2019). https://doi.org/10.5194/acp-19-11791-2019

Drury, E., Jacob, D. J., Spurr, R. J. D., Wang, J., Shinozuka, Y., Anderson, B.

E., Clarke, A. D., Dibb, J.,McNaughton, C., and Weber, R.: Synthesis of satellite (MODIS), aircraft (ICARTT), and surface (IMPROVE, EPA-AQS, AERONET) aerosol observations over eastern North America to improve MODIS aerosol retrievals and constrain surface aerosol concentrations andsources, Journal of Geophysical Research-Atmospheres, 115 (2010).
https://doi.org/10.1029/2009jd012629

Evans, M. J. and Jacob, D. J.: Impact of new laboratory studies of N2O5 hydrolysis on global model budgets of tropospheric nitrogen oxides, ozone, and OH, Geophysical Research Letters, 32 (2005).
https://doi.org/10.1029/2005gl022469

Eyring, V., Bony, S., Meehl, G. A., Senior, C. A., Stevens, B., Stouffer, R. J., and Taylor, K. E.: Overview of the Coupled Model Intercomparison Project Phase 6 (CMIP6) experimental design and organization, Geoscientific Model Development, 9, 1937-1958 (2016).
https://doi.org/10.5194/gmd-9-1937-2016

Fairlie, T. D., Jacob, D. J., and Park, R. J.: The impact of transpacific

transport of mineral dust in the United States, Atmospheric environment, 41, 1251-1266 (2007). https://doi.org/10.1016/j.atmosenv.2006.09.048

Fisher, J. A., Jacob, D. J., Wang, Q. Q., Bahreini, R., Carouge, C. C., Cubison, M. J., Dibb, J. E., Diehl, T., Jimenez, J. L., Leibensperger, E. M., Lu, Z. F., Meinders, M. B. J., Pye, H. O. T., Quinn, P. K., Sharma, S., Streets, D. G., van Donkelaar, A., and Yantosca, R. M.: Sources, distribution, and acidity of sulfate-ammonium aerosol in the Arctic in winter-spring, Atmospheric environment, 45, 7301-7318 (2011). https://doi.org/10.1016/j.atmosenv.2011.08.030

Forster, P., Ramaswamy, V., Artaxo, P., Berntsen, T., Betts, R., Fahey, D. W., Haywood, J., Lean, J., Lowe, D. C., and Myhre, G.: Changes in atmospheric constituents and in radiative forcing. Chapter 2. In: Climate Change 2007. The Physical Science Basis (2007).

Forster, P., Storelvmo, T., Armour, K., Collins, W., Dufresne, J.-L., Frame, D., Lunt, D. J., Mauritsen, T., Palmer, M. D., Watanabe, M., Wild, M., and Zhang, H.: The Earth's Energy Budget, Climate Feedbacks, and

Climate Sensitivity. In: Climate Change 2021: The Physical Science Basis, Cambridge University Press, In press.

Fountoukis, C. and Nenes, A.: ISORROPIA II: a computationally efficient thermodynamic equilibrium model for K+–Ca 2+–Mg 2+–NH 4+–Na+–SO 4 2−–NO 3−–Cl−–H 2 O aerosols, Atmospheric Chemistry and Physics, 7, 4639-4659 (2007). https://doi.org/10.5194/acp-7-4639-2007

Ginoux, P., Prospero, J. M., Torres, O., and Chin, M.: Long-term simulation of global dust distribution with the GOCART model: correlation with North Atlantic Oscillation, Environmental Modelling & Software, 19, 113-128 (2004). https://doi.org/10.1016/S1364-8152(03)00114-2

Guenther, A. B., Jiang, X., Heald, C. L., Sakulyanontvittaya, T., Duhl, T., Emmons, L. K., and Wang, X.: The Model of Emissions of Gases and Aerosols from Nature version 2.1 (MEGAN2.1): an extended and updated framework for modeling biogenic emissions, Geoscientific Model Development, 5, 1471-1492 (2012).

https://doi.org/10.5194/gmd-5-1471-2012

Gutman, G. and Ignatov, A.: The derivation of the green vegetation fraction from NOAA/AVHRR data for use in numerical weather prediction models, International Journal of Remote Sensing, 19, 1533-1543 (1998).

https://doi.org/10.1080/014311698215333

Han, J. and Pan, H. L.: Revision of Convection and Vertical Diffusion Schemes in the NCEP Global Forecast System, Weather and Forecasting, 26, 520-533 (2011).

https://doi.org/10.1175/Waf-D-10-05038.1

Han, J. Y., Hong, S. Y., and Kwon, Y. C.: The Performance of a Revised Simplified Arakawa-Schubert (SAS) Convection Scheme in the Medium-Range Forecasts of the Korean Integrated Model (KIM), Weather and Forecasting, 35, 1113-1128 (2020).

https://doi.org/10.1175/Waf-D-19-0219.1

Hansen, J., Sato, M., and Ruedy, R.: Radiative forcing and climate response, Journal of Geophysical Research-Atmospheres, 102, 6831-6864

(1997). https://doi.org/10.1029/96jd03436

Haywood, J. and Boucher, O.: Estimates of the direct and indirect radiative forcing due to tropospheric aerosols: A review, Reviews of Geophysics, 38, 513-543 (2000). https://doi.org/10.1029/1999rg000078

Hess, M., Koepke, P., and Schult, I.: Optical properties of aerosols and clouds: The software package OPAC, Bulletin of the American Meteorological Society, 79, 831-844 (1998). https://doi.org/10.1175/1520-0477(1998)079<0831:Opoaac>2.0.Co;2

Hong, S. Y., Kwon, Y. C., Kim, T. H., Kim, J. E. E., Choi, S. J., Kwon, I. H., Kim, J., Lee, E. H., Park, R. S., and Kim, D. I.: The Korean Integrated Model (KIM) System for Global Weather Forecasting, Asia-Pacific Journal of Atmospheric Sciences, 54, 267-292 (2018). https://doi.org/10.1007/s13143-018-0028-9

Hong, S. Y., Park, H., Cheong, H. B., Kim, J. E. E., Koo, M. S., Jang, J., Ham, S., Hwang, S. O., Park, B. K., Chang, E. C., and Li, H. Q.: The Global/Regional Integrated Model system (GRIMs), Asia-Pacific

Journal of Atmospheric Sciences, 49, 219-243 (2013). https://doi.org/10.1007/s13143-013-0023-0

Hsu, N. C., Tsay, S. C., King, M. D., and Herman, J. R.: Deep blue retrievals of Asian aerosol properties during ACE-Asia, IEEE Transactions on Geoscience and Remote Sensing, 44, 3180-3195 (2006). https://doi.org/10.1109/Tgrs.2006.879540

Intergovernmental Panel on Climate Change: Anthropogenic and Natural Radiative Forcing. In: Climate Change 2013 - The Physical Science Basis (2013).

Jacob, D. J.: Heterogeneous chemistry and tropospheric ozone, Atmospheric environment, 34, 2131-2159 (2000). https://doi.org/10.1016/S1352-2310(99)00462-8

Jacobson, M. Z.: Computation of Global Photochemistry with SMVGEAR-II, Atmospheric environment, 29, 2541-2546 (1995). https://doi.org/10.1016/1352-2310(95)00194-4

Jaeglé, L., Quinn, P., Bates, T., Alexander, B., and Lin, J.-T.: Global distribution of sea salt aerosols: new constraints from in situ and

remote sensing observations, Atmospheric Chemistry and Physics, 11, 3137-3157 (2011).
https://doi.org/10.5194/acp-11-3137-2011

Jeong, J. I. and Park, R. J.: Winter monsoon variability and its impact on aerosol concentrations in East Asia, Environ Pollut, 221, 285-292 (2017).
https://doi.org/10.1016/j.envpol.2016.11.075

Jeong, Y.-C., Yeh, S.-W., Lee, S., and Park, R. J.: A Global/Regional Integrated Model System-Chemistry Climate Model: 1. Simulation Characteristics, Earth and Space Science, 6, 2016-2030 (2019).
https://doi.org/10.1029/2019EA000727

Jo, D. S., Park, R. J., Lee, S., Kim, S. W., and Zhang, X. L.: A global simulation of brown carbon: implications for photochemistry and direct radiative effect, Atmospheric Chemistry and Physics, 16, 3413-3432 (2016).
https://doi.org/10.5194/acp-16-3413-2016

Kanamitsu, M., Ebisuzaki, W., Woollen, J., Yang, S. K., Hnilo, J. J., Fiorino,

M., and Potter, G. L.: NCEP-DOE AMIP-II reanalysis (R-2), Bulletin of the American Meteorological Society, 83, 1631-1643 (2002). https://doi.org/10.1175/BAMS-83-11-1631

Kim, M. J., Park, R. J., Ho, C. H., Woo, J. H., Choi, K. C., Song, C. K., and Lee, J. B.: Future ozone and oxidants change under the RCP scenarios, Atmospheric environment, 101, 103-115 (2015). https://doi.org/10.1016/j.atmosenv.2014.11.016

Koo, M.-S., Song, K., Kim, J.-E. E., Son, S.-W., Park, R. J., Chang, E.-C., Yeh, S.-W., Yoo, C., Jeong, J.-H., Moon, B.-K., Kim, H., and Hong, S.-Y.: The Global/Regional Integrated Model system (GRIMs): An update and seasonal evaluation, Asia-Pacific Journal of Atmospheric Sciences, To be submitted.

Kuhns, H., Knipping, E. M., and Vukovich, J. M.: Development of a United States-Mexico Emissions Inventory for the Big Bend Regional Aerosol and Visibility Observational (BRAVO) Study, J Air Waste Manag Assoc, 55, 677-692 (2005). https://doi.org/10.1080/10473289.2005.10464648

Lamarque, J. F., Bond, T. C., Eyring, V., Granier, C., Heil, A., Klimont, Z., Lee, D., Liousse, C., Mieville, A., Owen, B., Schultz, M. G., Shindell, D., Smith, S. J., Stehfest, E., Van Aardenne, J., Cooper, O. R., Kainuma, M., Mahowald, N., McConnell, J. R., Naik, V., Riahi, K., and van Vuuren, D. P.: Historical (1850-2000) gridded anthropogenic and biomass burning emissions of reactive gases and aerosols: methodology and application, Atmospheric Chemistry and Physics, 10, 7017-7039 (2010).
https://doi.org/10.5194/acp-10-7017-2010

Lamarque, J. F., Shindell, D. T., Josse, B., Young, P. J., Cionni, I., Eyring, V., Bergmann, D., Cameron-Smith, P., Collins, W. J., Doherty, R., Dalsoren, S., Faluvegi, G., Folberth, G., Ghan, S. J., Horowitz, L. W., Lee, Y. H., MacKenzie, I. A., Nagashima, T., Naik, V., Plummer, D., Righi, M., Rumbold, S. T., Schulz, M., Skeie, R. B., Stevenson, D. S., Strode, S., Sudo, K., Szopa, S., Voulgarakis, A., and Zeng, G.: The Atmospheric Chemistry and Climate Model Intercomparison Project (ACCMIP): overview and description of models, simulations and climate diagnostics, Geoscientific Model Development, 6, 179-206

(2013).

https://doi.org/10.5194/gmd-6-179-2013

Lee, J. W., Hong, S. Y., Chang, E. C., Suh, M. S., and Kang, H. S.: Assessment of future climate change over East Asia due to the RCP scenarios downscaled by GRIMs-RMP, Climate Dynamics, 42, 733-747 (2014).

https://doi.org/10.1007/s00382-013-1841-6

Levy, R. C., Mattoo, S., Munchak, L. A., Remer, L. A., Sayer, A. M., Patadia, F., and Hsu, N. C.: The Collection 6 MODIS aerosol products over land and ocean, Atmospheric Measurement Techniques, 6, 2989-3034 (2013).

https://doi.org/10.5194/amt-6-2989-2013

Lin, J. T. and McElroy, M. B.: Impacts of boundary layer mixing on pollutant vertical profiles in the lower troposphere: Implications to satellite remote sensing, Atmospheric environment, 44, 1726-1739 (2010).

https://doi.org/10.1016/j.atmosenv.2010.02.009

Lin, S. J. and Rood, R. B.: Multidimensional flux-form semi-Lagrangian transport schemes, Monthly Weather Review, 124, 2046-2070 (1996). https://doi.org/10.1175/1520-0493(1996)124<2046:Mffslt>2.0.Co;2

Liu, H., Jacob, D. J., Bey, I., and Yantosca, R. M.: Constraints from 210Pb and 7Be on wet deposition and transport in a global three-dimensional chemical tracer model driven by assimilated meteorological fields, Journal of Geophysical Research: Atmospheres, 106, 12109-12128 (2001). https://doi.org/10.1029/2000JD900839

Liu, H. Y., Crawford, J. H., Pierce, R. B., Norris, P., Platnick, S. E., Chen, G., Logan, J. A., Yantosca, R. M., Evans, M. J., Kittaka, C., Feng, Y., and Tie, X. X.: Radiative effect of clouds on tropospheric chemistry in a global three-dimensional chemical transport model, Journal of Geophysical Research-Atmospheres, 111 (2006). https://doi.org/10.1029/2005jd006403

Liu, M., Huang, X., Song, Y., Tang, J., Cao, J., Zhang, X., Zhang, Q., Wang, S., Xu, T., Kang, L., Cai, X., Zhang, H., Yang, F., Wang, H., Yu, J. Z.,

Lau, A. K. H., He, L., Huang, X., Duan, L., Ding, A., Xue, L., Gao, J., Liu, B., and Zhu, T.: Ammonia emission control in China would mitigate haze pollution and nitrogen deposition, but worsen acid rain, Proceedings of the National Academy of Sciences, 116, 7760-7765 (2019).
https://doi.org/doi:10.1073/pnas.1814880116

Liu, M., Huang, X., Song, Y., Xu, T., Wang, S., Wu, Z., Hu, M., Zhang, L., Zhang, Q., Pan, Y., Liu, X., and Zhu, T.: Rapid SO2 emission reductions significantly increase tropospheric ammonia concentrations over the North China Plain, Atmos. Chem. Phys., 18, 17933-17943 (2018).
https://doi.org/10.5194/acp-18-17933-2018

Lohmann, U. and Feichter, J.: Global indirect aerosol effects: a review, Atmospheric Chemistry and Physics, 5, 715-737 (2005).
https://doi.org/10.5194/acp-5-715-2005

Lohmann, U., Rotstayn, L., Storelvmo, T., Jones, A., Menon, S., Quaas, J., Ekman, A. M. L., Koch, D., and Ruedy, R.: Total aerosol effect:

radiative forcing or radiative flux perturbation?, Atmospheric Chemistry and Physics, 10, 3235-3246 (2010).
https://doi.org/10.5194/acp-10-3235-2010

Malm, W. C., Sisler, J. F., Huffman, D., Eldred, R. A., and Cahill, T. A.: Spatial and Seasonal Trends in Particle Concentration and Optical Extinction in the United-States, Journal of Geophysical Research-Atmospheres, 99, 1347-1370 (1994).
https://doi.org/10.1029/93jd02916

Malm, W. C., Schichtel, B. A., Pitchford, M. L., Ashbaugh, L. L., and Eldred, R. A.: Spatial and monthly trends in speciated fine particle concentration in the United States, Journal of Geophysical Research: Atmospheres, 109 (2004).
https://doi.org/https://doi.org/10.1029/2003JD003739

McLinden, C. A., Olsen, S. C., Hannegan, B., Wild, O., Prather, M. J., and Sundet, J.: Stratospheric ozone in 3-D models: A simple chemistry and the cross-tropopause flux, Journal of Geophysical Research-Atmospheres, 105, 14653-14665 (2000).

https://doi.org/10.1029/2000jd900124

Meinshausen, M., Smith, S. J., Calvin, K., Daniel, J. S., Kainuma, M. L. T., Lamarque, J. F., Matsumoto, K., Montzka, S. A., Raper, S. C. B., Riahi, K., Thomson, A., Velders, G. J. M., and van Vuuren, D. P. P.: The RCP greenhouse gas concentrations and their extensions from 1765 to 2300, Climatic Change, 109, 213 (2011). https://doi.org/10.1007/s10584-011-0156-z

Mishchenko, M. I., Travis, L. D., and Lacis, A. A.: Scattering, absorption, and emission of light by small particles, Cambridge university press (2002).

Mlawer, E. J., Taubman, S. J., Brown, P. D., Iacono, M. J., and Clough, S. A.: Radiative transfer for inhomogeneous atmospheres: RRTM, a validated correlated-k model for the longwave, Journal of Geophysical Research-Atmospheres, 102, 16663-16682 (1997). https://doi.org/10.1029/97jd00237

Monahan, E., Spiel, D., and Davidson, K.: A model of marine aerosol generation via whitecaps and wave disruption. In: Oceanic whitecaps,

Springer (1986).

Morgenstern, O., Hegglin, M. I., Rozanov, E., O'Connor, F. M., Abraham, N. L., Akiyoshi, H., Archibald, A. T., Bekki, S., Butchart, N., Chipperfield, M. P., Deushi, M., Dhomse, S. S., Garcia, R. R., Hardiman, S. C., Horowitz, L. W., Jockel, P., Josse, B., Kinnison, D., Lin, M. Y., Mancini, E., Manyin, M. E., Marchand, M., Marecal, V., Michou, M., Oman, L. D., Pitari, G., Plummer, D. A., Revell, L. E., Saint-Martin, D., Schofield,R., Stenke, A., Stone, K., Sudo, K., Tanaka, T. Y., Tilmes, S., Yamashita, Y., Yoshida, K., and Zeng, G.: Review of the global models used within phase 1 of the Chemistry-Climate Model Initiative (CCMI), Geoscientific Model Development, 10, 639-671 (2017).
https://doi.org/10.5194/gmd-10-639-2017

Murray, L. T., Jacob, D. J., Logan, J. A., Hudman,R. C., and Koshak, W. J.: Optimized regional and interannual variability of lightning in a global chemical transport model constrained by LIS/OTD satellite data, Journal of Geophysical Research-Atmospheres, 117 (2012).
https://doi.org/10.1029/2012jd017934

Myhre, G., Samset, B. H., Schulz, M., Balkanski, Y., Bauer, S., Berntsen, T. K., Bian, H., Bellouin, N., Chin, M., Diehl, T., Easter, R. C., Feichter, J., Ghan, S. J., Hauglustaine, D., Iversen, T., Kinne, S., Kirkevag, A., Lamarque, J. F., Lin, G., Liu, X., Lund, M. T., Luo, G., Ma, X., van Noije, T., Penner, J. E., Rasch, P. J., Ruiz, A., Seland,O., Skeie, R. B., Stier, P., Takemura, T., Tsigaridis, K., Wang, P., Wang, Z., Xu, L., Yu, H., Yu, F., Yoon, J. H., Zhang, K., Zhang, H., and Zhou, C.: Radiative forcing of the direct aerosol effect from AeroCom Phase II simulations, Atmospheric Chemistryand Physics, 13, 1853-1877 (2013).
https://doi.org/10.5194/acp-13-1853-2013

Naik, V., Horowitz, L. W., Fiore, A. M., Ginoux, P., Mao, J. Q., Aghedo, A. M., and Levy, H.: Impact of preindustrial to present-day changes in short-lived pollutant emissions on atmospheric composition and climate forcing, Journal of Geophysical Research-Atmospheres,118, 8086-8110 (2013).
https://doi.org/10.1002/jgrd.50608

Olivier, J. G., Bouwman, A., Berdowski, J.,Veldt, C., Bloos, J., Visschedijk,

A., Zandveld, P., and Haverlag, J.: Description of EDGAR Version 2.0: A set of global emission inventories of greenhouse gases and ozone-depleting substances for all anthropogenic and most natural sources on a per country basis and on 1 degree x 1 degree grid (1996).

Park, R. J., Jacob, D. J., Chin, M., and Martin, R. V.: Sources of carbonaceous aerosols over the United States and implications for natural visibility, Journal of Geophysical Research-Atmospheres, 108 (2003).
https://doi.org/10.1029/2002jd003190

Park, R. J., Jacob, D. J., Field, B. D., Yantosca, R. M., and Chin, M.: Natural and transboundary pollution influences on sulfate-nitrate-ammonium aerosols in the United States: Implications for policy, Journal of Geophysical Research-Atmospheres, 109 (2004).
https://doi.org/10.1029/2003jd004473

Pouyaei, A., Sadeghi, B., Choi, Y., Jung, J., Souri, A. H., Zhao, C., & Song, C. H.: Development and implementation of a physics-based convective mixing scheme in the community multiscale air quality

modeling framework, Journal of Advances in Modeling Earth Systems, 13 (2021).
https://doi.org/10.1029/2021MS002475

Pulles, T., van het Bolscher, M., Brand, R., and Visschedijk, A.: Assessment of global emissions from fuel combustion in the final decades of the 20th Century, TNO Rep. 2007-A-R0132B (2007).

Quaas, J., Ming, Y., Menon, S., Takemura, T., Wang, M., Penner, J. E., Gettelman, A., Lohmann, U., Bellouin, N., Boucher, O., Sayer, A. M., Thomas, G. E., McComiskey, A., Feingold, G., Hoose, C., Kristjansson, J. E., Liu, X., Balkanski, Y., Donner, L. J., Ginoux, P. A., Stier, P., Grandey, B., Feichter, J., Sednev, I., Bauer, S. E., Koch, D., Grainger, R. G., Kirkevag, A., Iversen, T., Seland, O., Easter, R., Ghan, S. J., Rasch, P. J., Morrison, H., Lamarque, J. F., Iacono, M. J., Kinne, S., and Schulz, M.: Aerosol indirect effects - general circulation model intercomparison and evaluation with satellite data, Atmospheric Chemistry and Physics, 9, 8697-8717 (2009).
https://doi.org/10.5194/acp-9-8697-2009

Rayner, N., Horton, E., Parker, D., Folland, C., and Hackett, R.: Version 2.2 of the global sea-ice and sea surface temperature data set, 1903–1994, Climate research technical note, 74, 43pp (1996).

Reichler, T., Dameris, M., and Sausen, R.: Determining the tropopause height from gridded data, Geophysical Research Letters, 30 (2003). https://doi.org/10.1029/2003gl018240

Remer, L. A., Kaufman, Y. J., Tanre, D., Mattoo, S., Chu, D. A., Martins, J. V., Li, R. R., Ichoku, C., Levy, R. C., Kleidman, R. G., Eck, T. F., Vermote, E., and Holben, B. N.: The MODIS aerosol algorithm, products, and validation, Journal of the atmospheric sciences, 62, 947-973 (2005). https://doi.org/10.1175/Jas3385.1

Sayer, A. M., Hsu, N. C., Bettenhausen, C., and Jeong, M. J.: Validation and uncertainty estimates for MODIS Collection 6 "Deep Blue" aerosol data, Journal of Geophysical Research-Atmospheres, 118, 7864-7872 (2013). https://doi.org/10.1002/jgrd.50600

Sheehan, P., Cheng, E., English, A., and Sun, F.: China's response to the air pollution shock, Nature Climate Change, 4, 306-309 (2014). https://doi.org/10.1038/nclimate2197

Shindell, D. T., Lamarque, J. F., Schulz, M., Flanner, M., Jiao, C., Chin, M., Young, P. J., Lee, Y. H., Rotstayn, L., Mahowald, N., Milly, G., Faluvegi, G., Balkanski, Y., Collins, W. J., Conley, A. J., Dalsoren, S., Easter, R., Ghan, S., Horowitz, L., Liu, X., Myhre, G., Nagashima, T., Naik, V., Rumbold, S. T., Skeie, R., Sudo, K., Szopa, S., Takemura, T., Voulgarakis, A., Yoon, J. H., and Lo, F.: Radiative forcing in the ACCMIP historical and future climate simulations, Atmospheric Chemistry and Physics, 13, 2939-2974 (2013). https://doi.org/10.5194/acp-13-2939-2013

Shindell, D. T., Levy, H., Schwarzkopf, M. D., Horowitz, L. W., Lamarque, J. F., and Faluvegi, G.: Multimodel projections of climate change from short-lived emissions due to human activities, Journal of Geophysical Research-Atmospheres, 113 (2008). https://doi.org/10.1029/2007jd009152

Sinyuk, A., Torres, O., and Dubovik, O.: Combined use of satellite and surface observations to infer the imaginary part of refractive index of Saharan dust, Geophysical Research Letters, 30 (2003). https://doi.org/10.1029/2002gl016189

Smith, S. J., van Aardenne, J., Klimont, Z., Andres, R. J., Volke, A., and Delgado Arias, S.: Anthropogenic sulfur dioxide emissions: 1850-2005, Atmos. Chem. Phys., 11, 1101-1116 (2011). https://doi.org/10.5194/acp-11-1101-2011

Stettler, M. E. J., Eastham, S., and Barrett, S. R. H.: Air quality and public health impacts of UK airports. Part I: Emissions, Atmospheric environment, 45, 5415-5424 (2011). https://doi.org/10.1016/j.atmosenv.2011.07.012

Stevenson, D., Dentener, F., Schultz, M., Ellingsen, K., Van Noije, T., Wild, O., Zeng, G., Amann, M., Atherton, C., and Bell, N.: Multimodel ensemble simulations of present-ay and near-future tropospheric ozone, Journal of Geophysical Research: Atmospheres, 111 (2006). https://doi.org/10.1029/2005JD006338

Stohl, A., Aamaas, B., Amann, M., Baker, L. H., Bellouin, N., Berntsen, T. K., Boucher, O., Cherian, R., Collins, W., Daskalakis, N., Dusinska, M., Eckhardt, S., Fuglestvedt, J. S., Harju, M., Heyes, C., Hodnebrog, O., Hao, J., Im, U., Kanakidou, M., Klimont, Z., Kupiainen, K., Law, K. S., Lund, M. T., Maas, R., MacIntosh, C. R., Myhre,G., Myriokefalitakis, S., Olivie, D., Quaas, J., Quennehen, B., Raut, J. C., Rumbold, S. T., Samset, B. H., Schulz, M., Seland, O., Shine, K. P., Skeie, R. B., Wang, S., Yttri, K. E., and Zhu, T.: Evaluating the climate and air quality impacts of short-lived pollutants, Atmospheric Chemistry and Physics, 15, 10529-10566 (2015). https://doi.org/10.5194/acp-15-10529-2015

Tao, W. K., Chen, J. P., Li, Z. Q., Wang, C., and Zhang, C. D.: Impact of Aerosols on Convective Clouds and Precipitation, Reviews of Geophysics, 50 (2012). https://doi.org/10.1029/2011rg000369

Tuccella, P., Curci, G., Visconti, G., Bessagnet, B., Menut, L., and Park, R. J.: Modeling of gas and aerosol with WRF/Chem over Europe: Evaluation and sensitivity study, Journal of Geophysical Research-

Atmospheres, 117 (2012).
https://doi.org/10.1029/2011jd016302

van der Werf, G. R., Randerson, J. T., Giglio, L., Collatz, G. J., Mu, M., Kasibhatla, P. S., Morton, D. C., DeFries, R. S., Jin, Y., and van Leeuwen, T. T.: Global fire emissions and the contribution of deforestation, savanna, forest, agricultural, and peat fires (1997–2009), Atmospheric Chemistry and Physics, 10, 11707-11735 (2010).
https://doi.org/10.5194/acp-10-11707-2010

van Donkelaar, A., Martin, R. V., Leaitch, W. R., Macdonald, A. M., Walker, T. W., Streets, D. G., Zhang, Q., Dunlea, E. J., Jimenez, J. L., Dibb, J. E., Huey, L. G., Weber, R., and Andreae, M. O.: Analysis of aircraft and satellite measurements from the Intercontinental Chemical Transport Experiment (INTEX-B) to quantify long-range transport of East Asian sulfur to Canada, Atmospheric Chemistry and Physics, 8, 2999-3014 (2008).
https://doi.org/10.5194/acp-8-2999-2008

Veefkind, J. P., de Haan, J. R., Brinksma, E. J., Kroon, M., and Levelt, P. F.:

Total ozone from the Ozone Monitoring Instrument (OMI) using the DOAS technique, IEEE Transactions on Geoscience and Remote Sensing, 44, 1239-1244 (2006). https://doi.org/10.1109/Tgrs.2006.871204

Walker, J. M., Philip, S., Martin, R. V., and Seinfeld, J. H.: Simulation of nitrate, sulfate, and ammonium aerosols over the United States, Atmospheric Chemistry and Physics, 12, 11213-11227 (2012). https://doi.org/10.5194/acp-12-11213-2012

Wang, J., Zhao, B., Wang, S., Yang, F., Xing, J., Morawska, L., Ding, A., Kulmala, M., Kerminen, V.-M., Kujansuu, J., Wang, Z., Ding, D., Zhang, X., Wang, H., Tian, M., Pet?j?, T., Jiang, J., and Hao, J.: Particulate matter pollution over China and the effects of control policies, Science of The Total Environment, 584-585, 426-447 (2017). https://doi.org/https://doi.org/10.1016/j.scitotenv.2017.01.027

Wesely, M. L.: Parameterization of Surface Resistances to Gaseous Dry Deposition in Regional-Scale Numerical-Models, Atmospheric environment, 23, 1293-1304 (1989).

https://doi.org/10.1016/0004-6981(89)90153-4

Wild, O., Zhu, X., and Prather, M. J.: Fast-j: Accurate simulation of in- and below-cloud photolysis in tropospheric chemical models, Journal of Atmospheric Chemistry, 37, 245-282 (2000).
https://doi.org/10.1023/A:1006415919030

Yienger, J. and Levy, H.: Empirical model of global soil-iogenic NOχ emissions, Journal of Geophysical Research: Atmospheres, 100, 11447-11464 (1995).
https://doi.org/10.1029/95JD00370

Young, P. J., Archibald, A. T., Bowman, K. W., Lamarque, J. F., Naik, V., Stevenson, D. S., Tilmes, S., Voulgarakis, A., Wild, O., Bergmann, D., Cameron-Smith, P., Cionni, I., Collins, W. J., Dalsoren, S. B., Doherty, R. M., Eyring, V., Faluvegi, G., Horowitz, L. W., Josse, B., Lee, Y. H., MacKenzie, I. A., Nagashima, T., Plummer,D. A., Righi, M., Rumbold, S. T., Skeie, R. B., Shindell, D. T., Strode, S. A., Sudo, K., Szopa, S., and Zeng, G.: Pre-industrial to end 21st century projections of tropospheric ozone from the Atmospheric Chemistry and Climate

Model Intercomparison Project (ACCMIP), Atmospheric Chemistry and Physics, 13, 2063-2090 (2013). https://doi.org/10.5194/acp-13-2063-2013

Zender, C. S., Bian, H. S., and Newman, D.: Mineral Dust Entrainment and Deposition (DEAD) model: Description and 1990s dust climatology, Journal of Geophysical Research-Atmospheres, 108 (2003). https://doi.org/10.1029/2002jd002775

Zhang, L., Jacob, D. J., Knipping, E. M., Kumar, N., Munger, J. W., Carouge, C. C., van Donkelaar, A., Wang, Y. X., and Chen, D.: Nitrogen deposition to the United States: distribution, sources, and processes, Atmospheric Chemistry and Physics, 12, 4539-4554 (2012). https://doi.org/10.5194/acp-12-4539-2012

Zhang, L. M., Gong, S. L., Padro, J., and Barrie, L.: A size-segregated particle dry deposition scheme for an atmospheric aerosol module, Atmospheric environment, 35, 549-560 (2001). https://doi.org/10.1016/S1352-2310(00)00326-5

Zhang, Q., Streets, D. G., Carmichael, G. R., He, K. B., Huo, H., Kannari,

A., Klimont, Z., Park, I. S., Reddy, S., Fu, J. S., Chen, D., Duan, L., Lei, Y., Wang, L. T., and Yao, Z. L.: Asian emissions in 2006 for the NASA INTEX-B mission, Atmospheric Chemistry and Physics, 9, 5131-5153 (2009).
https://doi.org/10.5194/acp-9-5131-2009

Zhang, Q., Jiang, X., Tong, D., Davis, S. J., Zhao, H., Geng, G., Feng, T., Zheng, B., Lu, Z., Streets, D. G., Ni, R., Brauer, M., van Donkelaar, A., Martin, R. V., Huo, H., Liu, Z., Pan, D., Kan, H., Yan, Y., Lin, J., He, K., and Guan, D.: Transboundary health impacts of transported global air pollution and international trade, Nature, 543, 705-709 (2017).
https://doi.org/10.1038/nature21712

Zheng, B., Tong, D., Li, M., Liu, F., Hong, C., Geng, G., Li, H., Li, X., Peng, L., Qi, J., Yan, L., Zhang, Y., Zhao, H., Zheng, Y., He, K., and Zhang, Q.: Trends in China's anthropogenic emissions since 2010 as the consequence of clean air actions, Atmos. Chem. Phys., 18, 14095-14111 (2018).
https://doi.org/10.5194/acp-18-14095-2018

국문 초록

GRIMs 전 지구 순환 모델과 GEOS-Chem 화학 수송 모델을 결합하여 새로운 화학-기후 모델인 Global/Regional Integrated Model system Chemistry Climate Model (GRIMs-CCM)을 개발하였다. GRIMs-CCM은 GRIMs에서 모의한 기상 변수들을 바탕으로 구동되며 화학 모듈에서 모의한 가스상 물질 및 에어로졸의 농도를 활용하여 복사 전달 방정식을 매 타임스텝 계산한다. 지상 네트워크에서 관측한 자료나 위성 관측 자료를 활용하여 모델의 오존 및 에어로졸 모의 성능을 검증하였다. 모델 검증 결과 GRIMs-CCM은 관측에서 나타난 연평균 에어로졸 광학두께의 전 지구적 공간분포를 성공적으로 모의하였고 연직 오존량의 계절적 변화와 위도에 따른 변화 또한 성공적으로 모의하였다. GRIMs-CCM에서 모의한 에어로졸 농도를 지상 관측 자료와 비교 검증한 결과 모델이 관측에서 나타난 에어로졸의 시공간 분포를 성공적으로 재현함을 확인하였으나 먼지 에어로졸의 농도를 관측보다 낮게 모의하였다. 또한 GRIMs-CCM을 활용하여 산업혁명 이전의 시기와 현재 시기의 10년 기후를 모의하고 그 차이를 비교함으로써

인간 활동에 따른 에어로졸 변화의 기후 효과를 산정하였다. GRIMs-CCM을 활용한 실험 결과에서는 산업혁명 이전의 시기부터 현재까지의 에어로졸 복사 강제력이 전구 평균 −0.30 W m^{-2}로 산정되었으며, 이는 다른 여러 기후 모델을 활용한 실험 결과에서 산정된 값과 유사한 결과이다. 이러한 결과는 GRIMs-CCM을 화학-기후 상호 작용에 관한 연구에 적절하게 활용할 수 있음을 제시하고 있다. 또한 GRIMs-CCM과 Community Earth System Model (CESM)을 활용한 기후 민감도 분석을 수행함으로써 동아시아 에어로졸의 지역적 기후 효과에 대하여 연구하였다. 최근 동아시아에서 감소하고 있는 에어로졸 광학 두께를 모델에 처방하여 20개의 앙상블 실험을 수행하였을 때 그 앙상블 평균이 ERA-Interim 재분석 자료에서 나타난 동아시아 겨울철 기온의 상승 추세를 성공적으로 재현함을 확인하였다. 에어로졸 광학 두께의 감소를 반영하지 않은 실험 결과와 비교하였을 때 에어로졸 광학 두께가 감소하는 실험에서 동아시아 기온 상승이 더 강하게 나타났고, 이를 통해 최근 동아시아 에어로졸의 감소가 동아시아 기온 상승에 부분적으로 기여하고 있음을 확인하였다.

주요어: 화학-기후 모형, 에어로졸, 오존, 에어로졸 복사 강제력,

GRIMs, GEOS-Chem

학 번: 2012-20345

감사의 글

박사학위 논문을 마무리하면서 길고도 길었던 대학원 생활을 돌이켜 보니 제 주변에 감사한 분들이 참 많다는 것을 새삼 느끼게 됩니다. 많은 분들이 저에게 힘이 되어 주셨고 격려와 조언을 아끼지 않았기에 부족한 제가 여기까지 올 수 있었습니다.

가장 먼저 저의 지도 교수님이신 박록진 교수님께 감사의 말씀을 드립니다. 교수님의 아낌없는 지도와 격려 덕분에 학위 과정을 잘 마무리할 수 있었습니다. 교수님은 항상 저의 롤 모델이셨습니다. 오랜 시간 교수님께 배우면서 훌륭한 연구자란 무엇인지 가까이서 보고 배울 수 있어서 너무 좋았습니다. 저도 교수님을 본받아 훌륭한 연구자가 될 수 있도록 노력하겠습니다. 그리고 바쁘심에도 불구하고 박사학위 논문 심사위원을 기꺼이 맡아 주시고 저의 학위논문이 잘 마무리될 수 있도록 도와주신 김상우 교수님, 손석우 교수님, 예상욱 교수님, 홍성유 교수님께 진심으로 감사드립니다.

학부와 대학원과정 동안 대기과학 전공수업을 들으면서 많은

교수님들께 가르침을 받았습니다. 학생들이 학문적 밑거름인 전공지식을 탄탄히 할 수 있도록 훌륭한 강의를 위해 힘써 주시고 또 대기과학 전공의 발전을 위해 힘써 주시는 지구환경과학부 대기과학 전공 모든 교수님들과 조교님들께 감사드립니다.

또 하나의 가족인 우리 대기화학모델링연구실 멤버들 모두 너무너무 감사합니다. 예리한 통찰력으로 연구에 대한 조언을 아낌없이 해주시는 정재인 박사님, 연구실에 없어서는 안 될 인간 비타민 유진이, 늘 징징대지만 그 모습조차 귀여운 귀염둥이 팀장 현민이, 수줍음이 많아서 얼굴이 빨개지면서도 재밌는 얘기를 많이 해주는 은조, 어떤 일을 맡겨도 훌륭하게 해낼 것 같은 믿음직스러운 기택이, 연구실의 살림꾼이자 정리정돈의 달인 시은이, 연구실 막내 분위기메이커 민아에게 감사드립니다. 우리 연구실의 화목한 가족 같은 분위기는 정말 다른 곳에 가서 자랑하고 싶을 정도로 최고라고 생각합니다. 연구실의 화목한 분위기 덕분에 오롯이 연구에 집중할 수 있었고 학위과정 동안 정말 행복했습니다. 그리고 졸업해서 지금 연구실에 계시지는 않지만 저와 학위과정을 함께했던 선후배님들도 너무너무 감사합니다. 독수리 오형제 멤버 민중이 형, 두성이 형, 승규 형, 형안이 형 모두 감사합니다.

형들과 함께 엠티도 가고 학회도 같이 다니고 연구도 같이 했던 기억들은 저에게 정말 잊을 수 없는 소중한 추억으로 남아있습니다. 그리고 늘 저를 응원해 주셨던 배수야 박사님과 구본양 박사님께도 정말 감사드립니다. 한 때 우리 연구실 홍일점이었던 한솔이, 천방지축이지만 항상 긍정적인 에너지가 넘치는 진결이, 못 하는게 없는 만능캐릭터 지수, 고양이박사 병현이 모두 너무너무 감사합니다.

그리고 사랑하는 우리 대학원 동기들, 아름 누나, 채윤 누나, 현호 형, 다솔이 모두 너무너무 감사합니다. 어려운 일이 있을 때 힘이 되어주고 서로 의지할 수 있는 동기들이 있어서 너무 좋았습니다. 그리고 501동 501A호 생활을 함께했던 상무 형과 유나에게도 감사합니다. 또 함께 연구 과제도 함께하고 공동세미나도 함께했던 기후환경연구실 멤버들을 비롯하여 501동 4층, 5층 대학원 생활을 함께 했던 모든 분들께 감사합니다.

SLCP 연구 과제를 수행하면서 만났던 인연들에게도 모두 감사합니다. 함께 과제 보고서도 작성하고 여러 행정적인 일로 고생했던 명일이, 지현이, 박수진 박사님, 위지은 박사님, 그리고 은승희 박사님께 감사드립니다. SLCP 연구 과제를 수행하면서 많은 도움을 주셨기에

5년간의 연구 과제를 마무리할 수 있었고 과제를 수행하면서 연구했던 내용들을 바탕으로 학위논문을 마무리할 수 있었습니다.

어렸을 때부터 인연을 이어온 소중한 친구들에게도 감사의 말씀을 드립니다. 정말 순수했던 초등학교 때 만나 학창 시절 대부분을 함께했고 지금은 맛있는 소고기집에서 만나 술 한 잔 기울이며 살아가는 얘기를 함께하는 호동이, 원중이, 원혁이에게 감사합니다. 그리고 3년간의 지옥의 고등학교 기숙사 생활을 함께하면서 서로 볼 꼴, 못 볼 꼴 다 본 사이인 민구, 유정이, 근형이를 포함한 영신고 3학년 8반 동기들에게 감사합니다.

사랑하는 우리 가족들 정말 감사합니다. 학위 과정동안 저를 위해 기도해 주시고 또 언제나 저를 믿어 주시고 격려해 주시고 응원해 주시는 어머니, 아버지 감사합니다. 학위 과정을 시작할 때만해도 철없는 동생이었던 것 같은데 어느새 어엿한 어른이 되어버린 것 같은 하나뿐인 동생 승철이에게도 감사합니다. 그리고 늘 저를 응원해 주셨지만 이제는 하늘나라에서 지켜보고 계실 할머니, 외할아버지, 막내 삼촌께도 감사드리고 지금도 저를 응원해주시고 지지해주시는 외할머니, 외삼촌, 이모, 서울 삼촌, 숙모, 막내 숙모, 고모, 고모부, 호경이 형,

원경이, 유민이, 채림이 모두 너무너무 감사드립니다.

그리고 마지막으로 학부생 때 만나 저의 길고 길었던 학위과정의 시작부터 끝까지 함께해준 사랑하는 유리에게 감사합니다. 그대는 박사과정 동안 가장 가까이서 가장 큰 힘이 되어주었고, 제가 심적으로 힘들 때마다 버텨내고 회복할 수 있는 정말 따뜻한 안식처가 되어주었습니다. 그대와 함께한 모든 순간이 정말 행복했고, 앞으로도 함께할 행복한 날들을 기대합니다. 정말 고맙고 사랑합니다.

한정된 지면에 일일이 언급하지는 못하였지만 지금까지 저에게 도움을 주셨던 모든 분들께 감사드립니다. 제가 받았던 도움을 평생 잊지 않고 항상 겸손한 자세로 학문에 정진하는, 다른 사람에게 도움이 되는 박사가 되겠습니다.